

DIVERGENCE-FREE DECOUPLED FINITE ELEMENT METHODS FOR INCOMPRESSIBLE FLOW PROBLEMS*

VOLKER JOHN [†], XU LI [‡], AND CHRISTIAN MERDON [§]

Abstract. Incompressible flows are modeled by a coupled system of partial differential equations for velocity and pressure. Starting from a divergence-free mixed method proposed in [John, Li, Mardon and Rui, Math. Models Methods Appl. Sci. 34(05):919–949, 2024], this paper proposes $\mathbf{H}(\text{div})$ -conforming finite element methods which decouple the velocity and pressure by constructing divergence-free basis functions. Algorithmic issues like the computation of this basis and the imposition of non-homogeneous Dirichlet boundary conditions are discussed. Numerical studies at two- and three-dimensional Stokes problems compare the efficiency of the proposed methods with methods from the above mentioned paper.

Key words. incompressible Stokes problem, decoupled methods, $\mathbf{H}(\text{div})$ -conforming finite element methods, divergence-free basis

AMS subject classifications. 65N12, 65N30, 76D07

1. Introduction. This paper is concerned with decoupled finite element methods for incompressible flow problems in a polyhedral domain $\Omega \subset \mathbb{R}^d$, $d \in \{2, 3\}$, with Lipschitz boundary. For the sake of concentrating on the main goal of this paper, the Stokes equations are considered

$$(1.1) \quad \begin{aligned} -\nu \Delta \mathbf{u} + \nabla p &= \mathbf{f} & \text{in } \Omega, \\ \text{div}(\mathbf{u}) &= 0 & \text{in } \Omega, \\ \mathbf{u} &= \mathbf{0} & \text{on } \partial\Omega, \end{aligned}$$

where the unknowns are the velocity \mathbf{u} and the pressure p , ν denotes the constant viscosity, and \mathbf{f} is the unit external body force.

The objective of this paper is to investigate a decoupled version of the Raviart–Thomas enriched Scott–Vogelius element method proposed in [22]. Scott–Vogelius elements are a class of well known and simple divergence-free elements (i.e., the discrete velocity solution is weakly divergence-free, which means that the $L^2(\Omega)$ norm of its divergence vanishes, cf. [34, 5, 38]), whose structure is exactly $\mathbf{P}_k \times \mathbf{P}_{k-1}^{\text{disc}}$, that is, the velocity space are classical k -th order Lagrange elements, while the pressure space consists of discontinuous piecewise polynomials of degree no more than $k-1$. As a class of divergence-free methods, it has many fascinating properties such as pressure-robustness (velocity error estimates are independent of the pressure, cf. [23]) and convection-robustness in the case of the Navier–Stokes equations (the constants in velocity error estimates do not depend on the Reynolds number, cf. [32, 12, 11]). However, the inf-sup stability of the classical Scott–Vogelius has severe requirements on the mesh and the polynomial degree (e.g., see [20]) especially in three dimensions (3D). This drawback was overcome in [22] by enriching the velocity space with some suitably chosen Raviart–Thomas bubbles.

It is well known that mixed methods for the Stokes equations result in a (non-positive definite) saddle point problem, while the decoupling of velocity and pressure only requires to solve several symmetric positive definite systems. Due to this reason, there is extensive literature studying decoupled methods such as the projection methods [35, 14, 18], consistent-splitting methods [15, 27, 19], and artificial com-

*

Funding: Xu Li was supported by NSFC (No. 12501511). Christian Mardon gratefully acknowledges the funding by the German Science Foundation (DFG) within the project “ME 4819/2-1”.

[†]Weierstrass Institute for Applied Analysis and Stochastics (WIAS), Anton-Wilhelm-Amo Str. 39, 10117 Berlin, Germany and Freie Universität Berlin, Department of Mathematics and Computer Science, Arnimallee 6, 14195 Berlin, Germany (john@wias-berlin.de).

[‡]School of Mathematics, Shandong University, Jinan 250100, China (xulisdu@sdu.edu.cn).

[§]Weierstrass Institute for Applied Analysis and Stochastics (WIAS), Anton-Wilhelm-Amo Str. 39, 10117 Berlin, Germany (merdon@wias-berlin.de).

pressibility methods [10, 16, 17]. These methods are efficient and the structure of their finite element spaces is usually very standard. However, these methods usually bypass the discretization of the continuity equation and thus they do not conserve mass exactly, i.e., the divergence of the computed velocity approximation usually does not vanish. Moreover, the stability analysis of these methods is much more technical than those of mixed methods and in some cases it is still an open problem. Another strategy consists in constructing divergence-free basis functions directly such as in [36] (see also the discretely divergence-free basis methods [37, 29]). However, the 3D basis functions in [36] are not linearly independent. In addition, to the best of the authors' knowledge, a robust strategy to deal with non-homogeneous boundary conditions for these classes of methods in 3D is an open problem. In [11], by reformulating the decoupled problem as a mixed Darcy system, the explicit construction of divergence-free basis functions is avoided, thereby circumventing the aforementioned difficulties. However, this approach requires the viscous and convective terms to be treated explicitly, and, unless hybrid-mixed elements are employed together with static condensation, one still needs to solve a saddle point problem.

On the first glance it seems to be very attractive to solve a problem for the velocity only, instead of a saddle point problem for velocity and pressure, because the saddle point character is removed and the number of degrees of freedom is reduced. This was our main motivation for developing divergence-free decoupled methods. The point of departure is the class of methods from [22]. First, a novel symmetric variant of these methods is proposed. Then, to construct a method with a divergence-free basis, a slight modification of the enrichment space is introduced. An appropriate decomposition of the space of discretely divergence-free functions is derived, which uses for the 3D situation a result and algorithm from [30]. The functions from this space are even weakly divergence-free. This decomposition offers a straightforward approach to define and implement weakly divergence-free basis functions. The imposition of non-homogeneous Dirichlet boundary conditions requires additional efforts. Depending on the concrete problem, different approaches can be pursued. In particular, a method is presented that works for arbitrary domains in two and three dimensions. The computation of a discrete approximation of the pressure is also discussed. Finally, the accuracy and efficiency of the proposed decoupled methods are studied by means of numerical comparisons with several methods proposed in [22]. These methods differ by the type of system (decoupled vs. saddle point), the sparsity (number of non-zero entries) and sparsity patterns of the arising matrices, and the overhead that is needed to compute the final solution.

This paper is organized as follows. In Section 2 we briefly introduce the Raviart–Thomas enriched Scott–Vogelius element method from [22] and a symmetric variant. The decoupled finite element method is proposed in Section 3. Two strategies to deal with non-homogeneous boundary conditions are discussed in Section 4, and a pressure reconstruction procedure, which is inspired by [15, 27], is given in Section 5. The numerical studies are presented in Section 6.

2. Notation and divergence-free mixed method from [22]. Standard notation for Lebesgue and Sobolev spaces is used. Vector-valued function spaces and functions are written with bold face symbols. The symbol (\cdot, \cdot) denotes the inner product in $L^2(\Omega)$ or $\mathbf{L}^2(\Omega)$.

The methods proposed in this paper are inspired from the methods developed in [22]. This section provides a brief description of the latter methods, it proposes a novel symmetric variant of these methods, and it introduces the finite element spaces used in this paper.

Denote $\mathbf{V} := \mathbf{H}_0^1(\Omega)$, $Q := L_0^2(\Omega)$, and let $\mathbf{f} \in \mathbf{L}^2(\Omega)$. A variational formulation of the Stokes equations with homogeneous velocity boundary conditions reads: Find $(\mathbf{u}, p) \in \mathbf{V} \times Q$ such that

$$\begin{aligned} (\nu \nabla \mathbf{u}, \nabla \mathbf{v}) - (\operatorname{div}(\mathbf{v}), p) &= (\mathbf{f}, \mathbf{v}) \quad \text{for all } \mathbf{v} \in \mathbf{V}, \\ (\operatorname{div}(\mathbf{u}), q) &= 0 \quad \text{for all } q \in Q. \end{aligned}$$

Let $\{\mathcal{T}_h\}$ be a family of admissible and shape-regular partitions of Ω . Let $\mathcal{T} \in \{\mathcal{T}_h\}$. A mesh cell of \mathcal{T} is denoted with T and the set of facets is denoted with \mathcal{F} . The symbols h_T and h_F are used to denote the diameter of $T \in \mathcal{T}$ and $F \in \mathcal{F}$, respectively. Let $h_{\mathcal{T}}$ be a piecewise constant function whose restriction on T equals h_T and set $h := \max_{T \in \mathcal{T}} h_T$.

The space of polynomials of degree k , $k \geq 0$, is denoted by $P_k(T)$. Following the notation in [22], the following finite element spaces are defined:

$$\begin{aligned} P_k(\mathcal{T}) &:= \{q_h \in H^1(\Omega) : q_h|_T \in P_k(T) \text{ for all } T \in \mathcal{T}\} \quad \text{for } k > 0, \\ P_k^{\text{disc}}(\mathcal{T}) &:= \{q_h \in L^2(\Omega) : q_h|_T \in P_k(T) \text{ for all } T \in \mathcal{T}\}, \\ \tilde{P}_k^{\text{disc}}(\mathcal{T}) &:= \{q_h \in P_k^{\text{disc}}(\mathcal{T}) : (q_h, 1)_T = 0 \text{ for all } T \in \mathcal{T}\}, \\ \mathbf{RT}_k(T) &:= \{\mathbf{v} \in \mathbf{L}^2(T) : \exists \mathbf{p} \in \mathbf{P}_k(T), q \in P_k(T), \mathbf{v}|_T(\mathbf{x}) = \mathbf{p}(\mathbf{x}) + q(\mathbf{x})\mathbf{x}\}, \\ \mathbf{RT}_k(\mathcal{T}) &:= \{\mathbf{v} \in \mathbf{H}(\text{div}, \Omega) : \forall T \in \mathcal{T} \mathbf{v}|_T \in \mathbf{RT}_k(T)\}, \end{aligned}$$

where $\mathbf{H}(\text{div}, \Omega)$ is the space of functions from $\mathbf{L}^2(\Omega)$ whose divergence is contained in $L^2(\Omega)$. The subspace of interior Raviart–Thomas cell functions reads

$$\mathbf{RT}_k^{\text{int}}(\mathcal{T}) := \{\mathbf{v} \in \mathbf{RT}_k(\mathcal{T}) : \mathbf{v} \cdot \mathbf{n}_T|_{\partial T} = 0 \text{ for all } T \in \mathcal{T}\}.$$

This space can be decomposed into

$$\mathbf{RT}_k^{\text{int}}(\mathcal{T}) = \mathbf{RT}_{k,0}^{\text{int}}(\mathcal{T}) \oplus \widetilde{\mathbf{RT}}_k^{\text{int}}(\mathcal{T}),$$

where $\mathbf{RT}_{k,0}^{\text{int}}(\mathcal{T})$ is the subspace of divergence-free Raviart–Thomas cell functions and $\widetilde{\mathbf{RT}}_k^{\text{int}}(\mathcal{T})$ is an arbitrary complement space to the former one. We require that all local spaces $\widetilde{\mathbf{RT}}_k^{\text{int}}(T)$ of $\widetilde{\mathbf{RT}}_k^{\text{int}}(\mathcal{T})$ come from the same reference space by Piola’s transformation, e.g., see [7, § 2.1].

The operator

$$\text{div}|_{\widetilde{\mathbf{RT}}_k^{\text{int}}(\mathcal{T})} : \widetilde{\mathbf{RT}}_k^{\text{int}}(\mathcal{T}) \rightarrow \tilde{P}_k^{\text{disc}}(\mathcal{T})$$

is a bijective operator, see [22] for an explanation of this property. Consequently there exists an inverse operator

$$(2.1) \quad \mathcal{R}_k : \tilde{P}_k^{\text{disc}}(\mathcal{T}) \rightarrow \widetilde{\mathbf{RT}}_k^{\text{int}}(\mathcal{T})$$

of $\text{div}|_{\widetilde{\mathbf{RT}}_k^{\text{int}}(\mathcal{T})}$ such that for any $q_h \in \tilde{P}_k^{\text{disc}}(\mathcal{T})$, it holds $\text{div}(\mathcal{R}_k q_h) = q_h$. We extend the definition of \mathcal{R}_k to Q by $\mathcal{R}_k q := \mathcal{R}_k(\pi_{\tilde{P}_k^{\text{disc}}(\mathcal{T})} q)$ such that $\text{div}(\mathcal{R}_k q) = \pi_{\tilde{P}_k^{\text{disc}}(\mathcal{T})} q$ for all $q \in Q$, where π_S is the $L^2(\Omega)$ projection to a space S .

Next, we recall the method developed and analyzed in [22]. For this purpose, define

$$\mathbf{V}_h^{\text{ct}} := \mathbf{P}_k(\mathcal{T}) \cap \mathbf{V}, \quad Q_h := P_{k-1}^{\text{disc}}(\mathcal{T}) \cap Q.$$

The pair of spaces $\mathbf{V}_h^{\text{ct}} \times Q_h$ is usually referred to as the Scott–Vogelius pair [33]. It is well known that in general Scott–Vogelius pairs do not satisfy a discrete inf-sup condition. A popular way to achieve an inf-sup stable discretization consists in enriching \mathbf{V}_h^{ct} with some suitable bubble functions, such as in the Bernardi–Raugel method [6] for $k = 1$. Instead of using \mathbf{H}^1 -conforming functions, it is advocated in [22] to utilize $\mathbf{H}(\text{div})$ -conforming Raviart–Thomas functions for enriching \mathbf{V}_h^{ct} . This approach does not require any integrals on facets and it leads in fact to a simple to implement method where the discrete velocity solution is weakly divergence-free. The fundamental principle for the choice of the enrichment space \mathbf{V}_h^{R} is summarized in the following.

For arbitrary k , there must be a subspace $\hat{Q}_h \subseteq Q_h$ so that $\mathbf{V}_h^{\text{ct}} \times \hat{Q}_h$ is inf-sup stable, e.g., $\hat{Q}_h = \{0\}$ is always a trivial choice for all k . For higher k , $k \geq d$, some classical inf-sup stable pairs on general shape-regular grids imply that $\mathbf{V}_h^{\text{ct}} \times (P_{k-d}^{\text{disc}}(\mathcal{T}) \cap Q)$ is inf-sup stable, cf. [13, pp. 132–144]. Hence any $\hat{Q}_h \subseteq (P_{k-d}^{\text{disc}}(\mathcal{T}) \cap Q)$ is an admissible choice in this situation. In some special cases \hat{Q}_h can be even equal

to Q_h , like in the case of Scott–Vogelius pairs on barycentrically refined grids for $k \geq d$, [5, 38]. Define $Q_h^0 := P_0^{\text{disc}}(\mathcal{T}) \cap Q$. It is required in [22] that

$$(2.2) \quad Q_h^0 \subseteq \hat{Q}_h \quad \text{for } k \geq d.$$

The finite element pressure space Q_h is split by $L^2(\Omega)$ -orthogonality as

$$Q_h = \hat{Q}_h \oplus_{L^2} \hat{Q}_h^\perp.$$

By (2.2), one has $\hat{Q}_h^\perp \subseteq \tilde{P}_{k-1}^{\text{disc}}(\mathcal{T})$ for $k \geq d$. Then, the principle for choosing \mathbf{V}_h^R consists in finding $\mathbf{V}_h^R \subseteq \mathbf{RT}_0(\mathcal{T}) \oplus \widetilde{\mathbf{RT}}_{k-1}^{\text{int}}(\mathcal{T})$ such that either

$$\text{div} : \mathbf{V}_h^R \rightarrow \hat{Q}_h^\perp \quad \text{is bijective for } k \geq d,$$

or

$$\text{div} : \mathbf{V}_h^R \rightarrow \hat{Q}_h^\perp \quad \text{is surjective for } k < d.$$

For more details, including some explicit constructions of \mathbf{V}_h^R , the reader is referred to [22].

Define the continuous space $\mathbf{V}(h) := \mathbf{V} \times \mathbf{V}_h^R$, the finite element space $\mathbf{V}_h := \mathbf{V}_h^{\text{ct}} \times \mathbf{V}_h^R$, and the bilinear forms

$$\begin{aligned} a &: \mathbf{V} \times \mathbf{V} \rightarrow \mathbb{R} & \text{by} & \quad a(\mathbf{u}^{\text{ct}}, \mathbf{v}^{\text{ct}}) := (\nabla \mathbf{u}^{\text{ct}}, \nabla \mathbf{v}^{\text{ct}}), \\ b &: \mathbf{V}(h) \times Q \rightarrow \mathbb{R} & \text{by} & \quad b(\mathbf{v}, q) := -(\text{div}(\mathbf{v}^{\text{ct}} + \mathbf{v}^R), q), \end{aligned}$$

for all $\mathbf{u} = (\mathbf{u}^{\text{ct}}, \mathbf{u}^R), \mathbf{v} = (\mathbf{v}^{\text{ct}}, \mathbf{v}^R) \in \mathbf{V}(h)$, and $q \in Q$. With an abuse of notation, for any $(\mathbf{v}, q) \in \mathbf{H}(\text{div}, \Omega) \times Q$, we define $b(\mathbf{v}, q) := -(\text{div}(\mathbf{v}), q)$.

The finite element method proposed in [22] reads as follows: Find $(\mathbf{u}_h, p_h) \in \mathbf{V}_h \times Q_h$ such that

$$(2.3) \quad \begin{aligned} \nu a_h(\mathbf{u}_h, \mathbf{v}_h) + b(\mathbf{v}_h, p_h) &= (\mathbf{f}, \mathbf{v}_h^{\text{ct}} + \mathbf{v}_h^R) \quad \text{for all } \mathbf{v}_h = (\mathbf{v}_h^{\text{ct}}, \mathbf{v}_h^R) \in \mathbf{V}_h, \\ b(\mathbf{u}_h, q_h) &= 0 \quad \text{for all } q_h \in Q_h, \end{aligned}$$

with

$$(2.4) \quad a_h(\mathbf{u}_h, \mathbf{v}_h) := a(\mathbf{u}_h^{\text{ct}}, \mathbf{v}_h^{\text{ct}}) - (\Delta_{\text{pw}} \mathbf{u}_h^{\text{ct}}, \mathbf{v}_h^R) + \delta (\Delta_{\text{pw}} \mathbf{v}_h^{\text{ct}}, \mathbf{u}_h^R) + a_h^S(\mathbf{u}_h^R, \mathbf{v}_h^R),$$

where Δ_{pw} is the piecewise Laplacian and $\delta = \pm 1$ selects the skew-symmetric variant of [22] (for $\delta = 1$) or the new symmetric variant (for $\delta = -1$). The stabilizing term is of the form

$$(2.5) \quad a_h^S(\mathbf{u}_h^R, \mathbf{v}_h^R) := a_h^D(\mathbf{u}_h^{\text{RT}0}, \mathbf{v}_h^{\text{RT}0}) + \frac{(1-\delta)\alpha}{2} (\text{div}(\tilde{\mathbf{u}}_h^R), \text{div}(\tilde{\mathbf{v}}_h^R)).$$

Here, $\mathbf{v}_h^{\text{RT}0}$ denotes the lowest order Raviart–Thomas part of $\mathbf{v}_h^R \in \mathbf{V}_h^R$ that only appears and needs to be stabilized in the case $k < d$, while $\tilde{\mathbf{v}}_h^R := \mathbf{v}_h^R - \mathbf{v}_h^{\text{RT}0}$ denotes the higher-order Raviart–Thomas enrichment of some $\mathbf{v}_h^R \in \mathbf{V}_h^R$ that only needs to be stabilized in the symmetric case $\delta = -1$. For the stabilization $a_h^D(\cdot, \cdot)$ three spectrally equivalent choices were suggested in [22, 25]. One of them, which is used in the numerical studies, is

$$(2.6) \quad a_h^D(\mathbf{u}_h^{\text{RT}0}, \mathbf{v}_h^{\text{RT}0}) := \alpha_0 \sum_{F \in \mathcal{F}^0} \text{dof}_F(\mathbf{u}_h^{\text{RT}0}) \text{dof}_F(\mathbf{v}_h^{\text{RT}0}) (\text{div} \psi_F, \text{div} \psi_F),$$

where $\text{dof}_F : \mathbf{H}^1(\Omega) + \mathbf{RT}_{k-1}(\mathcal{T}) \rightarrow \mathbb{R}$ evaluates the normal flux of the argument on the face F and the functions $\{\psi_F \in \mathbf{RT}_0(\mathcal{T}) : F \in \mathcal{F}\}$ form the standard basis of $\mathbf{RT}_0(\mathcal{T})$ such that

$$\mathbf{v}_h^{\text{RT}0} = \sum_{F \in \mathcal{F}} \text{dof}_F(\mathbf{v}_h^{\text{RT}0}) \psi_F = \sum_{F \in \mathcal{F}} \text{dof}_F(\mathbf{v}_h^R) \psi_F \quad \forall \mathbf{v}_h^R \in \mathbf{V}_h^R,$$

and the factors α and α_0 are parameters that allow to scale the stabilization and in [21] it was found that $\alpha_0 \approx 1$ is a good choice.

If $\delta = 1$, then $a_h(\cdot, \cdot)$ coincides with the bilinear form from the methods studied in [22]. If $\delta = -1$, then $a_h(\cdot, \cdot)$ is symmetric and positive definite whenever α and α_0 are sufficiently large. The newly introduced term is a stabilization of the $\widetilde{\mathbf{RT}}_{k-1}^{\text{int}}(\mathcal{T})$ part that is of magnitude $(h_{\mathcal{T}}^{-2} \tilde{\mathbf{u}}_h^R, \tilde{\mathbf{v}}_h^R)$. This statement can be proved using the inequality

$$\|\mathbf{v}_h\|_{L^2(T)} \leq Ch_T \|\operatorname{div}(\mathbf{v}_h)\|_{L^2(T)} \quad \text{for all } T \in \mathcal{T},$$

which is valid for all $\mathbf{v}_h \in \widetilde{\mathbf{RT}}_{k-1}^{\text{int}}(\mathcal{T})$, see [22, Lemma 5.2]. Method (2.3) will be called the full scheme.

Next, define

$$\widehat{\mathbf{V}}_h := \left\{ \mathbf{v}_h = (\mathbf{v}_h^{\text{ct}}, \mathbf{v}_h^R) \in \mathbf{V}_h : \operatorname{div}(\mathbf{v}_h^{\text{ct}} + \mathbf{v}_h^R) \in \widehat{Q}_h + Q_h^0 \right\},$$

and

$$(2.7) \quad \begin{aligned} \mathbf{V}_{h,0} &:= \left\{ \mathbf{v}_h = (\mathbf{v}_h^{\text{ct}}, \mathbf{v}_h^R) \in \mathbf{V}_h : b(\mathbf{v}_h, q_h) = 0 \text{ for all } q_h \in Q_h \right\} \\ &= \left\{ \mathbf{v}_h = (\mathbf{v}_h^{\text{ct}}, \mathbf{v}_h^R) \in \mathbf{V}_h : \operatorname{div}(\mathbf{v}_h^{\text{ct}} + \mathbf{v}_h^R) = 0 \right\} \subseteq \widehat{\mathbf{V}}_h. \end{aligned}$$

Note that $\widehat{Q}_h + Q_h^0 = \widehat{Q}_h$ for $k \geq d$ because of (2.2). Using the inverse of the divergence operator defined in (2.1), the operator

$$\mathcal{R}^{\perp} : \mathbf{V}_h^{\text{ct}} \rightarrow \mathbf{V}_h^R, \quad \mathcal{R}^{\perp} \mathbf{v}_h^{\text{ct}} := \mathcal{R}_{k-1} \pi_{\widehat{Q}_h^{\perp}} \operatorname{div}(\mathbf{v}_h^{\text{ct}}),$$

is defined. Hence it is $\operatorname{div}(\mathcal{R}^{\perp} \mathbf{v}_h^{\text{ct}}) = \pi_{\widehat{Q}_h^{\perp} \cap \widetilde{P}_{k-1}^{\text{disc}}(\mathcal{T})} \operatorname{div}(\mathbf{v}_h^{\text{ct}})$ and this allows to represent $\widehat{\mathbf{V}}_h$, for $k \geq d$, via

$$(2.8) \quad \widehat{\mathbf{V}}_h = \left\{ \mathbf{v}_h = (\mathbf{v}_h^{\text{ct}}, -\mathcal{R}^{\perp} \mathbf{v}_h^{\text{ct}}) : \mathbf{v}_h^{\text{ct}} \in \mathbf{V}_h^{\text{ct}} \right\},$$

see [22, Lemma 6.1].

For deriving a discrete problem that contains only the velocity, one first observes that the velocity solution of (2.3) is contained in $\widehat{\mathbf{V}}_h$, so that it is sufficient for the continuity constraint to consider test functions from $\widehat{Q}_h + Q_h^0$. Thus, for $k \geq d$, problem (2.3) is equivalent to finding $\mathbf{u}_h \in \widehat{\mathbf{V}}_h$ and $\hat{p}_h \in \widehat{Q}_h + Q_h^0$, such that

$$(2.9) \quad \begin{aligned} \nu a_h(\mathbf{u}_h, \mathbf{v}_h) + b(\mathbf{v}_h, \hat{p}_h) &= (\mathbf{f}, \mathbf{v}_h^{\text{ct}} + \mathbf{v}_h^R) \quad \text{for all } \mathbf{v}_h \in \widehat{\mathbf{V}}_h, \\ b(\mathbf{u}_h, q_h) &= 0 \quad \text{for all } q_h \in \widehat{Q}_h + Q_h^0, \end{aligned}$$

and, considering only the velocity, of seeking $\mathbf{u}_h \in \mathbf{V}_{h,0}$ such that

$$(2.10) \quad \nu a_h(\mathbf{u}_h, \mathbf{v}_h) = (\mathbf{f}, \mathbf{v}_h^{\text{ct}} + \mathbf{v}_h^R) \quad \text{for all } \mathbf{v}_h \in \mathbf{V}_{h,0}.$$

Using (2.8), problem (2.9) is also equivalent to computing $\mathbf{u}_h^{\text{ct}} \in \mathbf{V}_h^{\text{ct}}$ and $\hat{p}_h \in \widehat{Q}_h + Q_h^0$ such that

$$(2.11) \quad \begin{aligned} \nu a_h((\mathbf{u}_h^{\text{ct}}, -\mathcal{R}^{\perp} \mathbf{u}_h^{\text{ct}}), (\mathbf{v}_h^{\text{ct}}, -\mathcal{R}^{\perp} \mathbf{v}_h^{\text{ct}})) - (\operatorname{div}(\mathbf{v}_h^{\text{ct}}), \hat{p}_h) &= (\mathbf{f}, \mathbf{v}_h^{\text{ct}} - \mathcal{R}^{\perp} \mathbf{v}_h^{\text{ct}}) \quad \forall \mathbf{v}_h^{\text{ct}} \in \mathbf{V}_h^{\text{ct}}, \\ (\operatorname{div}(\mathbf{u}_h^{\text{ct}}), q_h) &= 0 \quad \forall q_h \in \widehat{Q}_h, \end{aligned}$$

for $k \geq d$. Since \mathcal{R}^{\perp} is an elementwise computable operator, see [22, Section 6], system (2.11) can be implemented easily and solved efficiently. Choosing \widehat{Q}_h as Q_h^0 results in a $\mathbf{P}_k \times P_0$ system, which will be called reduced scheme. For $k < d$ one can similarly obtain a $\mathbf{P}_k \oplus \mathbf{RT}_0 \times P_0$ system, see [22, Section 6.2] for more details. Therein a condensation method of the \mathbf{RT}_0 part is also discussed.

3. Finite element scheme for the velocity based on a divergence-free basis. The aim of the current paper is to construct appropriate pairs $\mathbf{V}_h \times Q_h$ in a slightly different framework such that the basis functions of $\mathbf{V}_{h,0}$ are easily computable. In this way, a decoupled computation of velocity and pressure is possible, where the velocity equation is given in (2.10). This approach is particularly appealing if only the velocity solution is needed. But even if in addition the pressure is of interest, it is not longer necessary to solve a discrete problem of saddle point character.

3.1. Derivation of the scheme. The new approach starts with a modification of the enrichment space of the full scheme (2.3). Let $\widetilde{\mathbf{RT}}_0 := \mathbf{RT}_0(\mathcal{T}) \cap \mathbf{H}_0(\text{div}, \Omega)$, where $\mathbf{H}_0(\text{div}, \Omega)$ is the subspace of functions from $\mathbf{H}(\text{div}, \Omega)$ with zero normal trace on $\partial\Omega$. Now, the original enrichment space \mathbf{V}_h^R is replaced with

$$\mathbf{V}_h^{\text{MR}} := \mathbf{V}_h^R + \widetilde{\mathbf{RT}}_0,$$

such that $\mathbf{V}_h^{\text{MR}} = \mathbf{V}_h^R$ for $k < d$ (see [22]) and $\mathbf{V}_h^{\text{MR}} = \mathbf{V}_h^R \oplus \widetilde{\mathbf{RT}}_0$ for $k \geq d$. By abuse of notation, we define $\mathbf{V}_h := \mathbf{V}_h^{\text{ct}} \times \mathbf{V}_h^{\text{MR}}$ and $\mathbf{V}(h) := \mathbf{V} \times \mathbf{V}_h^{\text{MR}}$.

For the moment, the new scheme can be written in form (2.3), with the modification mentioned above: Find $(\mathbf{u}_h, p_h) \in \mathbf{V}_h \times Q_h$, such that

$$(3.1) \quad \begin{aligned} \nu a_h(\mathbf{u}_h, \mathbf{v}_h) + b(\mathbf{v}_h, p_h) &= (\mathbf{f}, \mathbf{v}_h^{\text{ct}} + \mathbf{v}_h^R) & \text{for all } \mathbf{v}_h = (\mathbf{v}_h^{\text{ct}}, \mathbf{v}_h^R) \in \mathbf{V}_h, \\ b(\mathbf{u}_h, q_h) &= 0 & \text{for all } q_h \in Q_h. \end{aligned}$$

Next, a set of the computable basis functions of the (new) space $\mathbf{V}_{h,0}$ is derived and then the decoupling of velocity and pressure computation is performed. To this end, define

$$\mathbf{RT}_0^0 := \{\mathbf{v} \in \mathbf{RT}_0(\mathcal{T}) : \nabla \cdot \mathbf{v} = 0\}, \quad \widetilde{\mathbf{RT}}_0^0 := \left\{ \mathbf{v} \in \widetilde{\mathbf{RT}}_0 : \nabla \cdot \mathbf{v} = 0 \right\}.$$

Remark 3.1 (Basis for \mathbf{RT}_0^0). In the two-dimensional situation, it is known, e.g., see [4] and [36, Theorem 3.4], that

$$\mathbf{RT}_0^0 = \text{curl} (P_1(\mathcal{T}) \cap H^1(\Omega)/\mathbb{R}) \quad \text{and} \quad \widetilde{\mathbf{RT}}_0^0 = \text{curl} (P_1(\mathcal{T}) \cap H_0^1(\Omega)).$$

Moreover, the curl of the nodal basis of $P_1(\mathcal{T}) \cap H_0^1(\Omega)$ forms a basis for $\widetilde{\mathbf{RT}}_0^0$. In three dimensions, things become much more complicated due to the large kernel of the curl operator. In this case, \mathbf{RT}_0^0 and $\widetilde{\mathbf{RT}}_0^0$ are two subspaces of $\text{curl} \mathbf{N}_0$, with \mathbf{N}_0 being the lowest order Nédélec space, see [30]. In [30], the basis functions of \mathbf{N}_0 and some tools from graph theory are utilized for constructing linearly independent basis functions of \mathbf{RT}_0^0 and $\widetilde{\mathbf{RT}}_0^0$, which are also employed in our implementation of the proposed methods.

The following lemma shows a decomposition of the space of discretely divergence-free functions given by

$$\mathbf{V}_{h,0} := \{\mathbf{v}_h \in \mathbf{V}_h : b(\mathbf{v}_h, q_h) = 0 \text{ for all } q_h \in Q_h\}.$$

LEMMA 3.2 (Characterization of the space of discretely divergence-free functions). *It holds*

$$\mathbf{V}_{h,0} = \mathbf{V}_{h,0}^{\text{ct}} \oplus \left(\mathbf{0} \times \widetilde{\mathbf{RT}}_0^0 \right),$$

with

$$(3.2) \quad \mathbf{V}_{h,0}^{\text{ct}} := \text{span} \left\{ \left(\mathbf{v}_h^{\text{ct}}, -\mathcal{R}_{k-1} \text{div} (\mathbf{v}_h^{\text{ct}}) - \Pi_h^{\text{RT}_0} \mathbf{v}_h^{\text{ct}} \right) : \mathbf{v}_h^{\text{ct}} \in \mathbf{V}_h^{\text{ct}} \right\} \subset \mathbf{V}_h$$

and $\Pi_h^{\text{RT}_0}$ being the standard lowest-order Raviart–Thomas interpolation, i.e.,

$$\Pi_h^{\text{RT}_0} \mathbf{v}_h^{\text{ct}} := \sum_{F \in \mathcal{F}} \text{dof}_F(\mathbf{v}_h^{\text{ct}}) \boldsymbol{\psi}_F \quad \forall \mathbf{v}_h^{\text{ct}} \in \mathbf{V}_h^{\text{ct}}.$$

Proof. First it will be proved that $\mathbf{V}_{h,0}^{\text{ct}} \cap (\mathbf{0} \times \widetilde{\mathbf{RT}}_0^0) = \{\mathbf{0}\}$. For any $\mathbf{v}_h = (\mathbf{v}_h^{\text{ct}}, \mathbf{v}_h^{\text{R}}) \in \mathbf{V}_{h,0}^{\text{ct}} \cap (\mathbf{0} \times \widetilde{\mathbf{RT}}_0^0)$, we have $\mathbf{v}_h^{\text{ct}} = \mathbf{0}$ and hence also $\mathbf{v}_h^{\text{R}} = -\mathcal{R}_{k-1} \text{div}(\mathbf{v}_h^{\text{ct}}) - \Pi_h^{\text{RT}_0} \mathbf{v}_h^{\text{ct}} = \mathbf{0}$.

The next step consists in showing that $\mathbf{V}_{h,0}^{\text{ct}} \oplus (\mathbf{0} \times \widetilde{\mathbf{RT}}_0^0) \subseteq \mathbf{V}_{h,0}$. Let $\mathbf{v}_h^{\text{ct}} \in \mathbf{V}_h^{\text{ct}}$, then the definition of the extension of the inverse divergence operator (2.1) yields

$$\text{div}(\mathcal{R}_{k-1} \text{div}(\mathbf{v}_h^{\text{ct}})) = \pi_{\tilde{P}_{k-1}^{\text{disc}}(\mathcal{T})} \text{div}(\mathbf{v}_h^{\text{ct}})$$

and for the projection to $\mathbf{RT}_0(\mathcal{T})$ it is known that

$$\text{div}(\Pi_h^{\text{RT}_0} \mathbf{v}_h^{\text{ct}}) = \pi_{Q_h^0} \text{div}(\mathbf{v}_h^{\text{ct}}).$$

Since $\text{div}(\mathbf{v}_h^{\text{ct}}) \in P_{k-1}^{\text{disc}}(\mathcal{T}) \cap Q = \tilde{P}_{k-1}^{\text{disc}}(\mathcal{T}) \oplus_{L^2} Q_h^0$, it follows that $\text{div}(\mathbf{v}_h^{\text{ct}} - \mathcal{R}_{k-1} \text{div}(\mathbf{v}_h^{\text{ct}}) - \Pi_h^{\text{RT}_0} \mathbf{v}_h^{\text{ct}}) = 0$, which demonstrates that $\mathbf{V}_{h,0}^{\text{ct}} \oplus (\mathbf{0} \times \widetilde{\mathbf{RT}}_0^0) \subseteq \mathbf{V}_{h,0}$.

It remains to prove that $\mathbf{V}_{h,0} \subseteq \mathbf{V}_{h,0}^{\text{ct}} \oplus (\mathbf{0} \times \widetilde{\mathbf{RT}}_0^0)$. Consider an arbitrary $\mathbf{v}_h = (\mathbf{v}_h^{\text{ct}}, \mathbf{v}_h^{\text{R}}) \in \mathbf{V}_{h,0}$. Since it can be split as

$$\mathbf{v}_h = \left(\mathbf{v}_h^{\text{ct}}, -\mathcal{R}_{k-1} \text{div}(\mathbf{v}_h^{\text{ct}}) - \Pi_h^{\text{RT}_0} \mathbf{v}_h^{\text{ct}} \right) + \left(\mathbf{0}, \mathbf{v}_h^{\text{R}} + \mathcal{R}_{k-1} \text{div}(\mathbf{v}_h^{\text{ct}}) + \Pi_h^{\text{RT}_0} \mathbf{v}_h^{\text{ct}} \right),$$

it suffices to show that

$$(3.3) \quad \mathbf{v}_h^{\text{R}} + \mathcal{R}_{k-1} \text{div}(\mathbf{v}_h^{\text{ct}}) + \Pi_h^{\text{RT}_0} \mathbf{v}_h^{\text{ct}} \in \widetilde{\mathbf{RT}}_0^0.$$

By construction, the functions from $\mathbf{V}_{h,0}$ are even weakly divergence-free, since a property of the form (2.7) is valid also with the modified enrichment space. Using $\text{div}(\mathbf{v}_h^{\text{R}}) = -\text{div}(\mathbf{v}_h^{\text{ct}})$ and $\text{div}(\mathbf{v}_h^{\text{ct}}) \in P_{k-1}^{\text{disc}}(\mathcal{T})$ gives $\text{div}(\mathbf{v}_h^{\text{R}}) \in P_{k-1}^{\text{disc}}(\mathcal{T})$ and

$$\text{div}(\mathbf{v}_h^{\text{R}} + \mathcal{R}_{k-1} \text{div}(\mathbf{v}_h^{\text{ct}}) + \Pi_h^{\text{RT}_0} \mathbf{v}_h^{\text{ct}}) = \text{div}(\mathbf{v}_h^{\text{R}}) - \pi_{\tilde{P}_{k-1}^{\text{disc}}(\mathcal{T})} \text{div}(\mathbf{v}_h^{\text{R}}) - \pi_{P_0^{\text{disc}}(\mathcal{T})} \text{div}(\mathbf{v}_h^{\text{R}}) = 0.$$

In addition, it can be seen from this equation that $\text{div}(\mathbf{v}_h^{\text{R}} + \mathcal{R}_{k-1} \text{div}(\mathbf{v}_h^{\text{ct}})) \in Q_h^0$ (implying that the $\widetilde{\mathbf{RT}}_{k-1}^{\text{int}}(\mathcal{T})$ part of $\mathbf{v}_h^{\text{R}} + \mathcal{R}_{k-1} \text{div}(\mathbf{v}_h^{\text{ct}})$ vanishes), thus $\mathbf{v}_h^{\text{R}} + \mathcal{R}_{k-1} \text{div}(\mathbf{v}_h^{\text{ct}}) \in \widetilde{\mathbf{RT}}_0$ and hence the left-hand side of (3.3) is also a lowest order Raviart–Thomas function. Consequently (3.3) is shown. \square

Given the conforming velocity space \mathbf{V}_h^{ct} , then the representation of $\mathbf{V}_{h,0}$ in Lemma 3.2 offers a straightforward way to implement this space. The operators \mathcal{R}_{k-1} and $\Pi_h^{\text{RT}_0}$ are just cellwise and define a linear operator $\Pi^{\text{R}} : \mathbf{V}_h^{\text{ct}} \rightarrow \mathbf{V}_h^{\text{R}}$ given by

$$\Pi^{\text{R}} := -\mathcal{R}_{k-1} \text{div}(\mathbf{v}_h^{\text{ct}}) - \Pi_h^{\text{RT}_0} \mathbf{v}_h^{\text{ct}}$$

with a sparse matrix representation R . Altogether, this leads to the pressure-free formulation, which has the same velocity solution as (3.1): seek $(\mathbf{u}_h^{\text{ct}}, \mathbf{u}_h^{\text{RT}_0}) \in \mathbf{V}_h^{\text{ct}} \times \widetilde{\mathbf{RT}}_0^0$ such that

$$(3.4) \quad \nu a_h((\mathbf{u}_h^{\text{ct}}, \Pi^{\text{R}} \mathbf{u}_h^{\text{ct}} + \mathbf{u}_h^{\text{RT}_0}), (\mathbf{v}_h^{\text{ct}}, \Pi^{\text{R}} \mathbf{v}_h^{\text{ct}} + \mathbf{v}_h^{\text{RT}_0})) = (\mathbf{f}, \mathbf{v}_h^{\text{ct}} + \Pi^{\text{R}} \mathbf{v}_h^{\text{ct}} + \mathbf{v}_h^{\text{RT}_0})$$

for all $(\mathbf{v}_h^{\text{ct}}, \mathbf{v}_h^{\text{RT}_0}) \in \mathbf{V}_h^{\text{ct}} \times \widetilde{\mathbf{RT}}_0^0$. A basis for $\widetilde{\mathbf{RT}}_0^0$ is discussed in Remark 3.1 and we also consider the representation matrix S of the change of basis from $\widetilde{\mathbf{RT}}_0^0$ to \mathbf{RT}_0 .

Algebraically a linear system of the form

$$(3.5) \quad \begin{pmatrix} A^{\text{ct},\text{ct}} + A^{\text{ct},\text{R}} R + R^T A^{\text{R},\text{ct}} + R^T A^{\text{R},\text{R}} R & A^{\text{ct},\text{R}} S + R^T A^{\text{R},\text{R}} S \\ S^T A^{\text{R},\text{ct}} + S^T A^{\text{R},\text{R}} R & S^T A^{\text{R},\text{R}} S \end{pmatrix} \begin{pmatrix} \mathbf{x}^{\text{ct}} \\ \mathbf{x}^{\widetilde{\mathbf{RT}}_0^0} \end{pmatrix} = \begin{pmatrix} \mathbf{b}^{\text{ct}} + R^T \mathbf{b}^{\text{R}} \\ S^T \mathbf{b}^{\text{RT}_0} \end{pmatrix}$$

needs to be solved. Here, the A blocks represent the corresponding terms in (2.4) that also need to be implemented for the original method (3.1). The vectors \mathbf{b}^{ct} , \mathbf{b}^{R} , and \mathbf{b}^{RT_0} correspond to the evaluation of the right-hand side (\mathbf{f}, \bullet) in the basis functions of \mathbf{V}_h^{ct} , \mathbf{V}_h^{R} , and \mathbf{RT}_0 , respectively. Notice that, depending on δ , it holds either symmetry or skew-symmetry of A in the sense that $A^{\text{ct},\text{R}} = -\delta(A^{\text{R},\text{ct}})^T$.

3.2. Error estimate. The relationship between the cases $\delta = -1$ and $\delta = 1$ in (3.1) (or (3.4)) is very similar to the one between symmetric interior penalty Galerkin (SIPG) and nonsymmetric interior penalty Galerkin (NIPG), cf. [3]. Apart from the symmetry property, the primary difference between SIPG and NIPG is that, in SIPG, the penalty parameter must be chosen sufficiently large to guarantee stability (coercivity). On the other hand, the coercivity, boundedness, and consistency properties of a_h with $\delta = 1$ has been thoroughly analyzed in [22], although the velocity space therein is slightly different from the one in (3.1) when $k \geq d$. Therefore we only list some main results here and their proofs are omitted.

Define the norm $\| \cdot \|_\star$ on $\mathbf{V} \times \mathbf{V}_h^R$ as

$$\| \cdot \|_\star^2 := a_h(\mathbf{v}, \mathbf{v}) + \| h \Delta_{\text{pw}} \mathbf{v}^{\text{ct}} \|^2 + \| \text{div}(\tilde{\mathbf{v}}^R) \|^2,$$

for all $\mathbf{v} =: (\mathbf{v}^{\text{ct}}, \mathbf{v}^R) =: (\mathbf{v}^{\text{ct}}, \mathbf{v}^{\text{RT}_0} + \tilde{\mathbf{v}}^R) \in \mathbf{V} \times \mathbf{V}_h^R$.

LEMMA 3.3 (Properties of a_h). *Assume that the penalty parameter α in a_h is sufficiently large when $\delta = -1$. Then, the bilinear form a_h is coercive, bounded, and consistent in the sense that*

$$\begin{aligned} a_h(\mathbf{v}_h, \mathbf{v}_h) &\gtrsim \| \mathbf{v}_h \|_\star^2 && \text{for all } \mathbf{v}_h \in \mathbf{V}_{h,0}, \\ a_h(\mathbf{u}, \mathbf{v}) &\lesssim \| \mathbf{u} \|_\star \| \mathbf{v} \|_\star && \text{for all } \mathbf{u}, \mathbf{v} \in \mathbf{V} \times \mathbf{V}_h^R, \end{aligned}$$

and

$$\nu a_h((\mathbf{u}, \mathbf{0}), \mathbf{v}_h) = (\mathbf{f}, \mathbf{v}_h^{\text{ct}} + \mathbf{v}_h^R) \quad \text{for all } \mathbf{v}_h \in \mathbf{V}_{h,0},$$

respectively, where $\mathbf{u} \in \mathbf{V}$ is the velocity solution of (1.1).

In addition, since the velocity space used in our paper includes the one in [22], an inf-sup stability which is similar to [22, Theorem 4.1] is satisfied, i.e.,

$$\sup_{\mathbf{v}_h \in \mathbf{V}_h} \frac{b(\mathbf{v}_h, q_h)}{\| \mathbf{v}_h \|_\star} \geq \beta \| q_h \| \quad \text{for all } q_h \in Q_h,$$

where $\beta > 0$ is a constant independent of h .

The above properties, together with the approximation properties of \mathbf{V}_h^{ct} , e.g., see [8], yield the following error estimates, derived in the same way as in [22, Section 5].

THEOREM 3.4. *Let (\mathbf{u}, p) and (\mathbf{u}_h, p_h) be the solutions of (1.1) and (3.4), respectively, and consider a family of shape-regular triangulations $\{\mathcal{T}_h\}_{h>0}$. Assume that α is sufficiently large when $\delta = -1$ and $(\mathbf{u}, p) \in \mathbf{H}^{k+1}(\Omega) \times H^k(\Omega)$, then*

$$\| (\mathbf{u}, \mathbf{0}) - \mathbf{u}_h \|_\star \leq Ch^k |\mathbf{u}|_{\mathbf{H}^{k+1}(\Omega)},$$

where $C > 0$ is independent of h and ν .

4. Dealing with non-homogeneous boundary conditions. The incorporation of non-homogeneous Dirichlet boundary conditions in the proposed divergence-free decoupled methods is not straightforward. This section presents a simple approach, which is restricted to two-dimensional problems, and a general strategy suitable for two- and three-dimensional problems.

The discrete solution \mathbf{u}_h in the novel method can be split into three parts, compare the characterization of $\mathbf{V}_{h,0}$ in Lemma 3.2: The \mathbf{P}_k part (consider the first component of $\mathbf{V}_{h,0}^{\text{ct}}$), a divergence-free \mathbf{RT}_0 part (second part of $\mathbf{V}_{h,0}$), and a function in $\mathbf{RT}_{k-1}(\mathcal{T})$ (second component of $\mathbf{V}_{h,0}^{\text{ct}}$), whose divergence is exactly the additive inverse of the divergence of the \mathbf{P}_k part. Once the \mathbf{P}_k part is given, the third part of \mathbf{u}_h is also fixed, compare the definition (3.2) of $\mathbf{V}_{h,0}^{\text{ct}}$. When dealing with non-homogeneous boundary conditions, the \mathbf{P}_k boundary part can be defined by the usual interpolations/projections, and then the

third part is determined by it. Denoting the sum of these parts by $\mathbf{u}_h^{\text{ct+}}$, then it remains to determine a contribution $\check{\mathbf{u}}_h^{\text{R}}$ from the divergence-free \mathbf{RT}_0 part such that

$$\int_F (\mathbf{u}_h^{\text{ct+}} + \check{\mathbf{u}}_h^{\text{R}}) \cdot \mathbf{n} \, ds = \int_F \mathbf{u} \cdot \mathbf{n} \, ds \quad \text{for all } F \subset \partial\Omega.$$

This condition determines the degrees of freedom of $\check{\mathbf{u}}_h^{\text{R}}$ on each facet at the boundary.

Altogether, the task of imposing non-homogeneous Dirichlet boundary conditions is reduced to the following general problem: For any function g on $\partial\Omega$, find an inexpensive strategy to get a function $\mathbf{z}_h \in \mathbf{RT}_0^0$ such that $\int_F \mathbf{z}_h \cdot \mathbf{n} \, ds = \int_F g \, ds$ for all $F \subset \partial\Omega$. This function can be used to impose the boundary values of the divergence-free \mathbf{RT}_0 part. Having decomposed in this way $\check{\mathbf{u}}_h^{\text{R}} = \check{\mathbf{u}}_h^{\text{R}} + \mathbf{z}_h$, where $\check{\mathbf{u}}_h^{\text{R}} \in \widetilde{\mathbf{RT}}_0^0$ takes homogeneous boundary conditions, leads to a change of the right-hand side in (3.5) to

$$\begin{pmatrix} \mathbf{b}^{\text{ct}} + R^T \mathbf{b}^{\text{R}} - A^{\text{ct,R}} \mathbf{x}_z \\ S^T \mathbf{b}^{\text{RT}_0} - S^T A^{\text{R,R}} \mathbf{x}_z \end{pmatrix},$$

where \mathbf{x}_z are the coefficients of \mathbf{z}_h w.r.t. the \mathbf{RT}_0 basis (hence a transform of the basis via S does not appear). After having solved the modified system (3.5), one needs to add \mathbf{z}_h to its solution.

Below two strategies for the construction of \mathbf{z}_h are discussed.

4.1. A simple strategy in two dimensions. A simple strategy to deal with non-homogeneous boundary conditions in two dimensions was proposed in [36, Sect. 3.3]. Note that for any $\mathbf{z}_h = \text{curl} \phi_h$ with $\phi_h \in P_1(\mathcal{T})$, the tangential derivative satisfies $\partial \phi_h / \partial \tau = \mathbf{z}_h \cdot \mathbf{n}$, and thus

$$\phi_h(\mathbf{x}) = \phi_h(\mathbf{x}_0) + \int_{\mathbf{x}_0}^{\mathbf{x}} \mathbf{z}_h \cdot \mathbf{n} \, ds, \quad \mathbf{x} \in \partial\Omega,$$

where both $\mathbf{x}_0 \in \partial\Omega$ and $\phi_h(\mathbf{x}_0)$ are arbitrary. Thus, fixing a vertex \mathbf{x}_0 at some component of $\partial\Omega$ and a value $\phi_h(\mathbf{x}_0)$ determines the value of ϕ_h at all other vertices at this boundary component. After having computed in this way values at all vertices on each component of $\partial\Omega$, one can assign some value to each vertex in Ω , e.g., zero, defining in this way ϕ_h and then \mathbf{z}_h can be computed.

4.2. A robust strategy for both two- and three-dimensional spaces. For any function g on $\partial\Omega$, consider the following problem: Find $(\mathbf{z}_h, r_h) \in \mathbf{RT}_0(\mathcal{T}) \times Q_h^0$ such that

$$(4.1) \quad \int_F \mathbf{z}_h \cdot \mathbf{n} \, ds = \int_F g \, ds \quad \text{for all } F \subset \partial\Omega,$$

$$(4.2) \quad D_h(\mathbf{z}_h, \mathbf{v}_h) - (r_h, \text{div}(\mathbf{v}_h)) + (\text{div}(\mathbf{z}_h), q_h) = 0 \quad \text{for all } (\mathbf{v}_h, q_h) \in \widetilde{\mathbf{RT}}_0 \times Q_h^0,$$

where

$$D_h(\mathbf{z}_h, \mathbf{v}_h) := \sum_{F \in \mathcal{F}} \text{dof}_F(\mathbf{z}_h) \text{dof}_F(\mathbf{v}_h) (\psi_F, \psi_F).$$

In [25] it is proved that $D_h(\bullet, \bullet)$ and (\bullet, \bullet) are spectrally equivalent on $\mathbf{RT}_0(\mathcal{T})$, which, together with the inf-sup stability of $\widetilde{\mathbf{RT}}_0 \times Q_h^0$ (cf. [7]), guarantees the unique solvability of the Darcy-type problem (4.1). Notice that the matrix from D_h is diagonal with positive entries on its diagonal. Hence, one obtains a symmetric positive definite (s.p.d.) Schur complement matrix and one could compute r_h by using a solver for s.p.d. systems. And since D_h is a diagonal matrix, one can obtain thereafter \mathbf{z}_h locally from r_h . Clearly we have $\mathbf{z}_h \in \mathbf{RT}_0^0$.

Computing the boundary values by solving (4.1) requires the solution of a global Darcy-type problem, which is not efficient. A much more efficient approach is solving a similar problem on a much smaller subdomain near the boundary. Define

$$\mathcal{T}_\partial = \{T \in \mathcal{T} : \partial T \cap \partial\Omega \neq \emptyset\},$$

that is, \mathcal{T}_∂ is the union of all vertex patches (see, e.g., [24]) of the boundary vertices and let $\Omega_\partial = \cup_{T \in \mathcal{T}_\partial} T$. Then, the following much smaller system also provides a solution with the desired properties: Find $(\mathbf{z}_h, r_h) \in \mathbf{RT}_0(\mathcal{T}_\partial) \times (P_0^{\text{disc}}(\mathcal{T}_\partial) \cap L_0^2(\Omega_\partial))$ such that

$$(4.3) \quad \int_F \mathbf{z}_h \cdot \mathbf{n} \, d\mathbf{s} = \int_F g \, d\mathbf{s} \quad \text{for all } F \subset \partial\Omega,$$

$$(4.4) \quad \int_F \mathbf{z}_h \cdot \mathbf{n} \, d\mathbf{s} = 0 \quad \text{for all } F \subset \partial\Omega_\partial \setminus \partial\Omega,$$

$$(4.5) \quad D_h(\mathbf{z}_h, \mathbf{v}_h) - (r_h, \text{div}(\mathbf{v}_h)) + (\text{div}(\mathbf{z}_h), q_h) = 0 \quad \text{for all } (\mathbf{v}_h, q_h) \in (\mathbf{RT}_0(\mathcal{T}_\partial) \cap \mathbf{H}_0(\text{div}, \Omega_\partial)) \\ \times (P_0^{\text{disc}}(\mathcal{T}_\partial) \cap L_0^2(\Omega_\partial)).$$

If Ω is simply connected, Ω_∂ must be a connected domain. Then the inf-sup stability of the pair $(\mathbf{RT}_0(\mathcal{T}_\partial) \cap \mathbf{H}_0(\text{div}, \Omega_\partial)) \times (P_0^{\text{disc}}(\mathcal{T}_\partial) \cap L_0^2(\Omega_\partial))$ can be guaranteed, too. Thus (4.3)–(4.5) is a well-posed problem. If Ω is multiply connected, Ω_∂ can be disconnected (consisting of several connected components). In this case one just needs to solve several independent systems like (4.3)–(4.5).

5. Computing the discrete pressure. In many situations the pressure solution is also important. Here we discuss one strategy to approximate the pressure, which is inspired by a class of consistent splitting schemes proposed in [15, 27]. It seeks a pressure solution in $H^1(\Omega)/\mathbb{R}$. It relies on the identity $\Delta \mathbf{u} = \nabla(\nabla \cdot \mathbf{u}) - \nabla \times (\nabla \times \mathbf{u})$ which allows to replace the Laplacian in (1.1) by the curl-curl operator. Then, testing the momentum with ∇q for any $q \in H^1(\Omega)$ yields

$$(5.1) \quad (\nabla p, \nabla q) = -(\nu \nabla \times \nabla \times \mathbf{u}, \nabla q) + (\mathbf{f}, \nabla q) = \nu \int_{\partial\Omega} (\nabla \times \mathbf{u}) \cdot (\mathbf{n} \times \nabla q) \, d\mathbf{s} + (\mathbf{f}, \nabla q).$$

This leads to the following pressure reconstruction scheme: Find $p_h \in P_\ell(\mathcal{T}) \cap H^1(\Omega) \cap Q$ with $\ell \geq 1$ such that

$$(5.2) \quad (\nabla p_h, \nabla q_h) = (\mathbf{f}, \nabla q_h) + \nu \int_{\partial\Omega} (\nabla \times \mathbf{u}_h^{\text{ct}}) \cdot (\mathbf{n} \times \nabla q_h) \, d\mathbf{s} \quad \text{for all } q_h \in P_\ell(\mathcal{T}) \cap H^1(\Omega) \cap Q,$$

which is a pure Neumann problem with inhomogeneous boundary conditions. The solution can be computed by utilizing a solver for s.p.d. systems. Notice that the finite element pressure reconstruction computed with (5.2) substitutes the finite element pressure which is present in (3.1) and which then disappears in the derivation of the method with divergence-free velocity basis. For the sake of simplifying the notation in the presentation of the numerical results, we use the notation p_h also for the reconstructed discrete pressure.

THEOREM 5.1. *Under the assumption that a quasi-uniform family of triangulations $\{\mathcal{T}_h\}_{h>0}$ is considered, the error of p_h computed by (5.2) can be bounded by*

$$(5.3) \quad \|\nabla(p - p_h)\|_{L^2(\Omega)} \leq \inf_{q_h \in P_\ell(\mathcal{T}_h) \cap H^1(\Omega) \cap Q} \|\nabla(p - q_h)\|_{L^2(\Omega)} + \nu Ch^{k-1} \|\mathbf{u}\|_{\mathbf{H}^{k+1}(\Omega)},$$

where $C > 0$ is independent of h and ν .

Proof. Let $\Pi_h p \in P_\ell(\mathcal{T}_h) \cap H^1(\Omega) \cap Q$ be the Riesz projection (best approximation with respect to $H^1(\Omega)$) of p . Using this projection, the error equation obtained by subtracting (5.2) from (5.1) with test function $q_h = \Pi_h p - p_h$ gives

$$(5.4) \quad \|\nabla(\Pi_h p - p_h)\|_{L^2(\Omega)}^2 = (\nabla(p - p_h), \nabla(\Pi_h p - p_h)) = \nu \int_{\partial\Omega} (\nabla \times (\mathbf{u} - \mathbf{u}_h^{\text{ct}})) \cdot (\mathbf{n} \times \nabla(\Pi_h p - p_h)) \, d\mathbf{s}.$$

Consider the following auxiliary problem: Find $e_{p,S} \in Q$ such that

$$(\nabla e_{p,S}, \nabla q) = \int_{\partial\Omega} (\nabla \times (\mathbf{u} - \mathbf{u}_h^{\text{ct}})) \cdot (\mathbf{n} \times \nabla q) \, ds$$

for all $q \in Q$. Then (5.4) implies

$$\|\nabla(\Pi_h p - p_h)\|_{L^2(\Omega)}^2 = \nu(\nabla e_{p,S}, \nabla(\Pi_h p - p_h)) \leq \nu \|\nabla e_{p,S}\|_{L^2(\Omega)} \|\nabla(\Pi_h p - p_h)\|_{L^2(\Omega)},$$

and further

$$\|\nabla(\Pi_h p - p_h)\|_{L^2(\Omega)} \leq \nu \|\nabla e_{p,S}\|_{L^2(\Omega)}.$$

Indeed, $e_{p,S}$ is the Stokes pressure corresponding to $\mathbf{u} - \mathbf{u}_h^{\text{ct}}$ and it satisfies the estimate, see [27, 26],

$$\begin{aligned} (5.5) \quad \|\nabla e_{p,S}\|_{L^2(\Omega)}^2 &\leq C_\varepsilon \|\nabla(\mathbf{u} - \mathbf{u}_h^{\text{ct}})\|_{L^2(\Omega)}^2 + \left(\frac{1}{2} + \varepsilon\right) \|\Delta_{\text{pw}}(\mathbf{u} - \mathbf{u}_h^{\text{ct}})\|_{L^2(\Omega)}^2 \\ &\quad + C \sum_{F \in \mathcal{F}^0} h_F^{-1} \int_F |\llbracket \nabla(\mathbf{u} - \mathbf{u}_h^{\text{ct}}) \rrbracket|^2 \, ds, \end{aligned}$$

where ε can be arbitrarily small, $C_\varepsilon > 0$ depends on ε^{-1} , and $\llbracket \cdot \rrbracket$ denotes the jump operator on facets whose definition can be found in [26]. Under the quasi-uniformity assumption, it follows from [8, Theorem 1.6.6] and Young's inequality that

$$(5.6) \quad \sum_{F \in \mathcal{F}^0} h_F^{-1} \int_F |\llbracket \nabla(\mathbf{u} - \mathbf{u}_h^{\text{ct}}) \rrbracket|^2 \, ds \leq C \left(h^{-2} \|\nabla(\mathbf{u} - \mathbf{u}_h^{\text{ct}})\|_{L^2(\Omega)}^2 + \sum_{T \in \mathcal{T}_h} \|\nabla(\mathbf{u} - \mathbf{u}_h^{\text{ct}})\|_{H^1(T)}^2 \right).$$

Let $\mathcal{I}\mathbf{u}$ be an interpolation of \mathbf{u} satisfying [8, Eq. (4.4.5)]. By successively applying the triangle inequality, the inverse inequality, and again the triangle inequality, one obtains

$$\begin{aligned} \|\nabla(\mathbf{u} - \mathbf{u}_h^{\text{ct}})\|_{H^1(T)} &\leq \|\nabla(\mathbf{u} - \mathcal{I}\mathbf{u})\|_{H^1(T)} + \|\nabla(\mathcal{I}\mathbf{u} - \mathbf{u}_h^{\text{ct}})\|_{H^1(T)} \\ &\leq \|\nabla(\mathbf{u} - \mathcal{I}\mathbf{u})\|_{H^1(T)} + Ch^{-1} \|\nabla(\mathcal{I}\mathbf{u} - \mathbf{u}_h^{\text{ct}})\|_{L^2(T)} \\ &\leq \|\nabla(\mathbf{u} - \mathcal{I}\mathbf{u})\|_{H^1(T)} + Ch^{-1} \|\nabla(\mathbf{u} - \mathcal{I}\mathbf{u})\|_{L^2(T)} + Ch^{-1} \|\nabla(\mathbf{u} - \mathbf{u}_h^{\text{ct}})\|_{L^2(T)}, \end{aligned}$$

which, together with Theorem 3.4, implies

$$\sum_{T \in \mathcal{T}_h} \|\nabla(\mathbf{u} - \mathbf{u}_h^{\text{ct}})\|_{H^1(T)}^2 \leq Ch^{2k-2} \|\mathbf{u}\|_{\mathbf{H}^{k+1}(\Omega)}^2,$$

and further, by utilizing (5.5) and (5.6), one obtains

$$\|\nabla e_{p,S}\|_{L^2(\Omega)}^2 \leq Ch^{2k-2} \|\mathbf{u}\|_{\mathbf{H}^{k+1}(\Omega)}^2.$$

The Pythagorean identity

$$\|\nabla(p - p_h)\|_{L^2(\Omega)}^2 = \|\nabla(p - \Pi_h p)\|_{L^2(\Omega)}^2 + \|\nabla(\Pi_h p - p_h)\|_{L^2(\Omega)}^2.$$

concludes the proof. \square

Theorem 5.1 shows that the pressure error is also optimal if one chooses $\ell \leq k - 1$.

Notice that the usual norm of the error analysis for the pressure in mixed finite element methods is the $L^2(\Omega)$ norm and not the $L^2(\Omega)$ norm of the gradient as in Theorem 5.1. The proof in mixed methods uses the discrete inf-sup condition for the bilinear form that couples the velocity and pressure finite element spaces. However, there is no such bilinear form in the decoupled method as a consequence of using divergence-free velocity basis functions. We think that it is possible to derive an estimate for the $L^2(\Omega)$ error of the reconstructed pressure utilizing the Aubin–Nitsche trick and expect convergence of one order higher than in (5.3) for sufficiently smooth data. However, this is outside the scope of this paper.

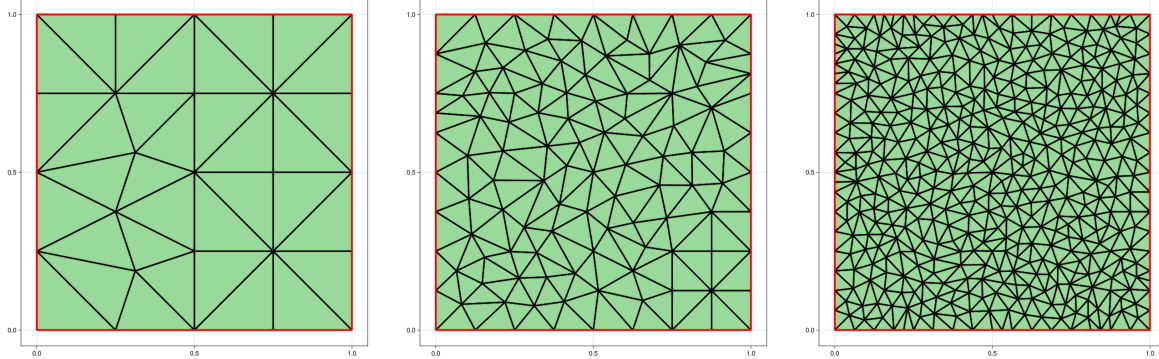


Fig. 1: Example 6.1. The first three computational grids.

6. Numerical studies. The objectives of this section are twofold. First, the expectations concerning the convergence of the decoupled methods should be supported, e.g., compare Theorem 3.4, where the velocity approximation was computed by solving (3.4) and the pressure approximation as described in Section 5. And second, the efficiency of these methods shall be compared with those of the full mixed method from [22], see (2.3), and the reduced mixed method from [22], see (2.11). Using a decoupled approach seems to be on the first glance more efficient than having to solve a saddle point problem, which was one of our main motivation for constructing the new methods. However, also other aspects possess an impact on the efficiency, like the sparsity pattern of the arising matrices and the number of non-zero entries (nnz). The considered methods differ in these aspects. In addition, the decoupled methods and the reduced mixed method need additional overhead to compute the final solution. For the decoupled method, this overhead consists of constructing the divergence-free basis, of incorporating non-homogeneous Dirichlet boundary conditions, and of computing the pressure (if needed).

All methods have been implemented in the code [28]. For solving the linear systems of equations, the sparse direct solver Pardiso [31, 9] was used, where we set `iparm` 8 to the value 10, `iparm` 10 to the value 6 for the two-dimensional simulations and the value 8 for the three-dimensional ones, `iparm` 11 to the value 1, and `iparm` 13 to 0 for the polynomial degree $k = 1$ and for the skew-symmetric case in three dimensions, and otherwise to the value 1. For the special case $k = d = 3$, we changed `iparm` 8 to the value 4 and `iparm` 10 to the value 11.

The stabilization parameter α in (2.5) is set to $\alpha = 100$ in $d = 2$ dimensions and to $\alpha = 200$ in $d = 3$ dimensions. For the special case $k = d = 3$ the stabilization parameter is set $\alpha = 300$. The stabilization parameter $\alpha_0 = 1$ is used in (2.6) for the lowest order schemes $k = 1$ according to the experience in [21] and for the skew-symmetric case ($\delta = 1$) in $d = 3$ dimensions. In the higher order ($k > 1$) and symmetric case ($\delta = -1$), $\alpha_0 = \alpha$ is used.

Notice that for polynomial degree $k = 1$ the terms with δ vanish for all methods. We present the corresponding results together with the symmetric variants of the methods.

6.1. A two-dimensional example. This example is given by $\Omega = (0, 1)^2$ and the right-hand side and Dirichlet boundary conditions are set such that

$$\mathbf{u}(x, y) := \begin{pmatrix} -\partial_y \xi \\ \partial_x \xi \end{pmatrix} \quad \text{where} \quad \xi = -\sin(2\pi x) \cos(2\pi y), \quad p := \frac{\cos(4\pi x) - \cos(4\pi y)}{4}$$

satisfy the Stokes problem for $\nu = 1$ or $\nu = 10^{-6}$, respectively.

Simulations were performed on a sequence of unstructured grids with decreasing mesh width, where the first three grids are depicted in Figure 1, and for different polynomial degrees, up to $k = 4$. The

Table 1: Example 6.1. Number of degrees of freedom (ndofs) and number of non-zero sparse matrix entries (nnz) of the full system for the decoupled method with divergence-free basis (dfb), the reduced mixed method (red), and the full mixed method (full) for different orders k and $\delta = 1$ (skew-symmetric case).

level	ndofs dfb (k=2)	ndofs red (k=2)	ndofs full (k=2)	nnz dfb (k=2)	nnz red (k=2)	nnz full (k=2)
1	196	204	340	4152	3954	4588
2	961	1040	1816	25761	22990	30008
3	3829	4194	7426	106975	95380	126734
4	14744	16265	29037	418918	375183	500821
5	57805	63997	114721	1656779	1486953	1990197
level	ndofs dfb (k=3)	ndofs red (k=3)	ndofs full (k=3)	nnz dfb (k=3)	nnz red (k=3)	nnz full (k=3)
1	382	390	662	12588	12182	18574
2	1965	2044	3596	74355	68232	108096
3	7945	8310	14774	309561	282480	450990
4	30858	32379	57923	1218462	1112093	1781891
5	121505	127697	229145	4831089	4408413	7076425
level	ndofs dfb (k=4)	ndofs red (k=4)	ndofs full (k=4)	nnz dfb (k=4)	nnz red (k=4)	nnz full (k=4)
1	636	644	1086	29958	28314	43886
2	3357	3436	5958	171319	159246	253858
3	13677	14042	24546	711305	660364	1058620
4	53358	54879	96388	2801492	2602693	4183050

non-homogeneous Dirichlet boundary conditions were imposed for the decoupled methods as described in Section 4.1. Information on the number of degrees of freedom and the non-zero entries for the different methods are provided in Tables 1 and 2. In case of the decoupled schemes, the numbers only include the degrees of freedom or nonzero entries for the velocity problem, the decoupled (and smaller) pressure problem is not included. As it was a motivation of the construction of the decoupled methods with divergence-free basis, the number of degrees of freedom is smallest for this method. The corresponding numbers for the reduced methods are usually a bit larger and the full mixed methods have often around twice as many degrees of freedom than the corresponding decoupled methods. The situation is somewhat different with respect to the number of non-zero matrix entries, since these numbers are often similar for the decoupled methods and the corresponding reduced mixed methods. The most non-zero entries are usually required by the full mixed methods.

The convergence of the studied methods in the large viscosity case $\nu = 1$ is illustrated in Figures 2 and 3 for the skew-symmetric and the symmetric case, respectively. One can observe that all methods show the expected orders of convergence. The velocity errors for all the methods are virtually the same. The proposed pressure reconstruction for the decoupled methods leads often to results of superior accuracy compared to those obtained with the mixed methods. With respect to the velocity, similar observations can be made in the small viscosity case $\nu = 10^{-6}$, compare Figures 4 and 5. The velocity errors are of the same order of magnitude as for the large viscosity case. The latter observation supports the pressure-robustness of the methods. Interestingly, the pressure reconstruction used in the decoupled methods leads on finer grids consistently to noticeably more accurate discrete pressures than those computed with the mixed methods.

Figures 6–9 provide information about the efficiency of the studied methods in terms of computing times, using the direct sparse solver. As expected by construction, the reduced mixed methods are always more efficient than the full mixed methods. Also the decoupled methods with divergence-free velocity basis are always faster than the full mixed methods. In some situations, the simulations with the decoupled methods were even somewhat faster than with the reduced mixed methods, sometimes both

Table 2: Example 6.1. Number of degrees of freedom (ndofs) and number of non-zero sparse matrix entries (nnz) of the full system for the decoupled method with divergence-free basis (dfb), the reduced mixed method (red), and the full mixed method (full) for different orders k and $\delta = -1$ (symmetric case).

level	ndofs dfb (k=1)	ndofs red (k=1)	ndofs full (k=1)	nnz dfb (k=1)	nnz red (k=1)	nnz full (k=1)
1	78	86	145	980	676	853
2	345	424	732	6201	4404	5328
3	1329	1694	2944	25847	18566	22316
4	5016	6537	11401	101328	73393	87985
5	19467	25659	44828	400971	291609	349116
6	77094	102213	178727	1603802	1168725	1398267
7	306741	407826	713404	6411081	4676514	5593248
level	ndofs dfb (k=2)	ndofs red (k=2)	ndofs full (k=2)	nnz dfb (k=2)	nnz red (k=2)	nnz full (k=2)
1	196	204	340	4564	3994	4656
2	961	1040	1816	26597	23008	30396
3	3829	4194	7426	109871	95382	128350
4	14744	16265	29037	430134	375227	507207
5	57805	63997	114721	1700653	1486965	2015559
level	ndofs dfb (k=3)	ndofs red (k=3)	ndofs full (k=3)	nnz dfb (k=3)	nnz red (k=3)	nnz full (k=3)
1	382	390	662	13058	12182	18778
2	1965	2044	3596	75469	68232	109260
3	7945	8310	14774	313051	282480	455838
4	30858	32379	57923	1230714	1112093	1801049
5	121505	127697	229145	4875581	4408413	7152511
level	ndofs dfb (k=4)	ndofs red (k=4)	ndofs full (k=4)	nnz dfb (k=4)	nnz red (k=4)	nnz full (k=4)
1	636	644	1086	30100	28314	44294
2	3357	3436	5958	171949	159246	256186
3	13677	14042	24546	713821	660364	1068316
4	53358	54879	96388	2811244	2602693	4221366

approaches are of the same efficiency, and in the other cases the reduced mixed methods were a little bit faster. Altogether, the presented results show the good efficiency of both, the decoupled and the reduced mixed methods. We observe that, in the symmetric cases, which are of particular interest in practice, the decoupled methods are often a bit faster than the reduced mixed methods.

6.2. A three-dimensional example. This example considers a Stokes problem in $\Omega = (0, 1)^3$ with $\nu = 1$ and the prescribed solution

$$\mathbf{u}(x, y, z) = \operatorname{curl}(\sin(y), \cos(z), \sin(x))^T, \quad p(x, y, z) = \frac{\cos(4\pi x) - \cos(4\pi y)}{4},$$

which determines the right-hand side \mathbf{f} and the Dirichlet boundary condition on $\partial\Omega$.

Numerical results are presented only for the reduced mixed methods and the decoupled methods with divergence-free velocity basis. The simulations considered a sequence of unstructured grids with decreasing mesh width, see Figure 10 for the three coarsest grids, and polynomials up to degree $k = 3$. To impose the non-homogeneous Dirichlet boundary condition in the decoupled methods, the method that restricts the Darcy-type problem to a subdomain close to the boundary, see the end of Section 4.2, was applied. The number of degrees of freedom and non-zero matrix entries is given in Tables 3 and 4. It can be observed that usually both, the numbers of degrees of freedom and the numbers of non-zero entries, are smaller for the reduced methods, except $k = 2$. For $k = 2$, the situation with respect to the non-zero matrix entries is vice versa.

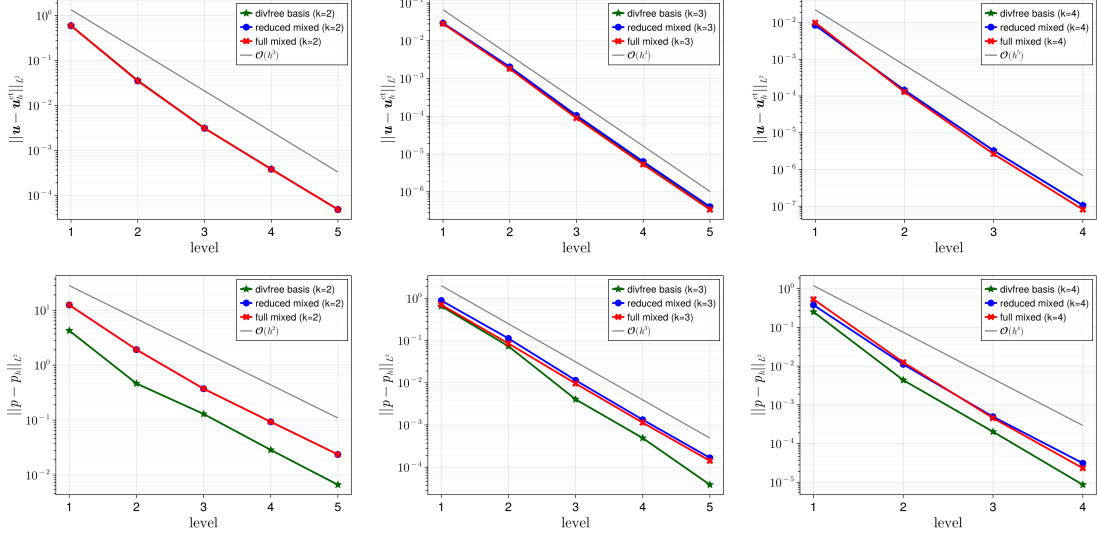


Fig. 2: Example 6.1 with $\nu = 1$. $L^2(\Omega)$ velocity error (top) and pressure error (bottom) for the polynomial degree $k = 2$ (left), $k = 3$ (center), and $k = 4$ (right), $\delta = 1$ (skew-symmetric case).

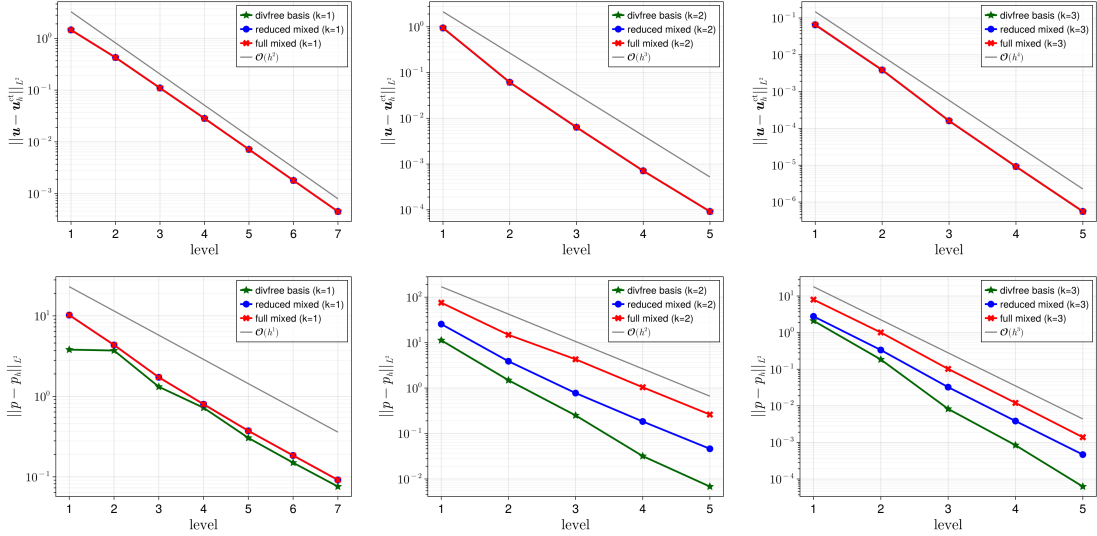


Fig. 3: Example 6.1 with $\nu = 1$. $L^2(\Omega)$ velocity error (top) and pressure error (bottom) for the polynomial degree $k = 1$ (left), $k = 2$ (center), and $k = 3$ (right), $\delta = -1$ (symmetric case).

The behavior of velocity and pressure errors is depicted in Figures 11 and 12. Like in the two-dimensional example, the velocity errors computed with both methods are virtually the same, while the pressure approximations for the decoupled methods show a better accuracy than those computed with the reduced mixed methods.

Finally, computing times are provided in Figures 13 and 14. In most cases, the reduced mixed

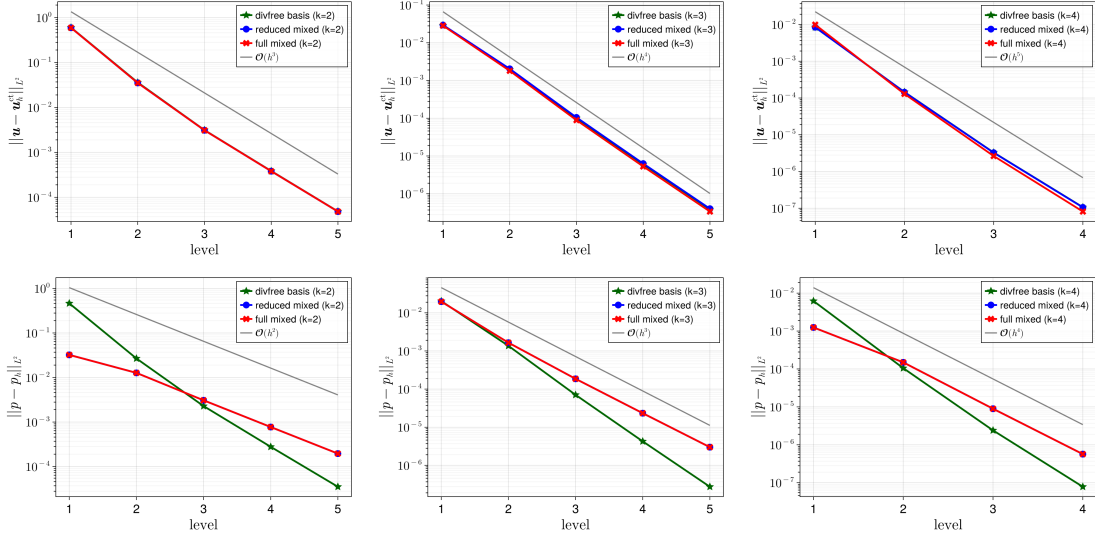


Fig. 4: Example 6.1 with $\nu = 10^{-6}$. $L^2(\Omega)$ velocity error (top) and pressure error (bottom) for the polynomial degree $k = 1$ (left), $k = 2$ (center), and $k = 3$ (right), $\delta = 1$ (skew-symmetric case).

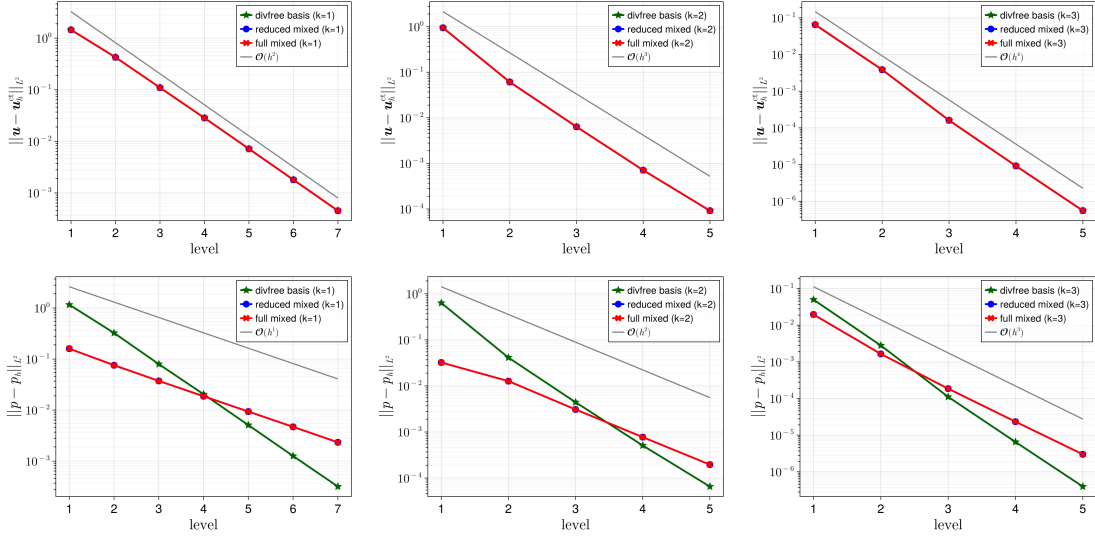


Fig. 5: Example 6.1 with $\nu = 10^{-6}$. $L^2(\Omega)$ velocity error (top) and pressure error (bottom) for the polynomial degree $k = 2$ (left), $k = 3$ (center), and $k = 4$ (right), $\delta = -1$ (symmetric case).

methods are somewhat faster than the decoupled methods. However, for $k = 2$, which is a very common choice in practice, the decoupled methods are more efficient.

7. Summary and outlook. This paper proposed finite element methods for the incompressible Stokes equations with a basis of the velocity space consisting of divergence-free functions. In this way, it is possible to compute the velocity approximation without needing to solve a coupled velocity-pressure

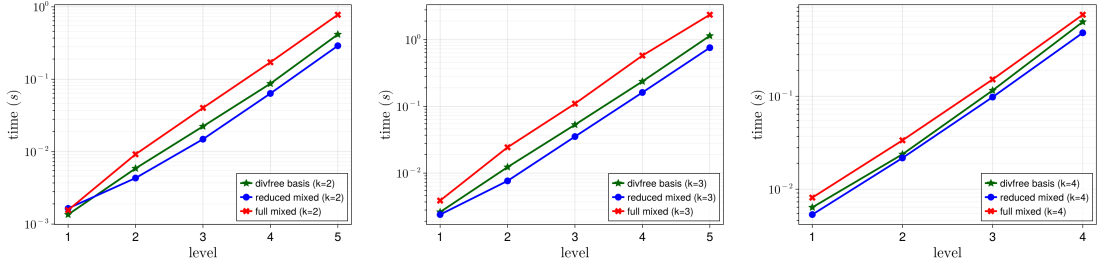


Fig. 6: Example 6.1 with $\nu = 1$. Solver times with Pardiso for polynomial degree $k = 2$ (left), $k = 3$ (center), and $k = 4$ (right), $\delta = 1$ (skew-symmetric case).

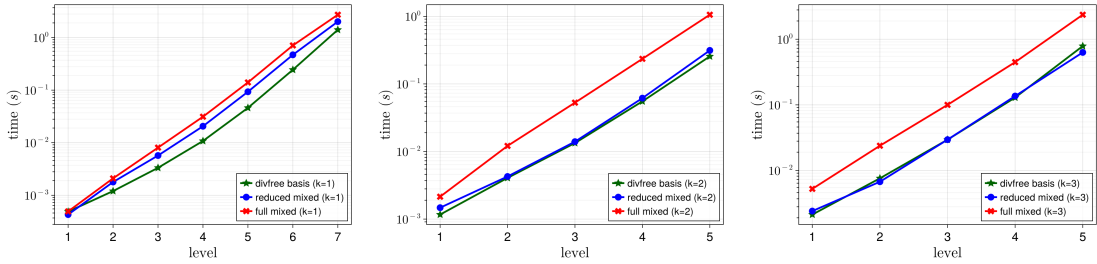


Fig. 7: Example 6.1 with $\nu = 1$. Solver times with Pardiso for polynomial degree $k = 1$ (left), $k = 2$ (center), and $k = 3$ (right), $\delta = -1$ (symmetric case).

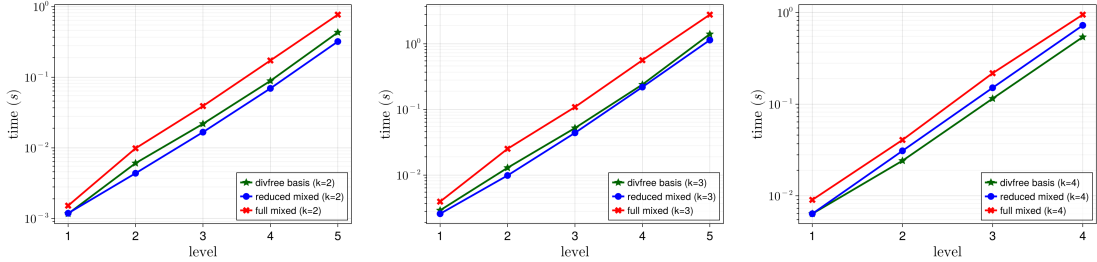


Fig. 8: Example 6.1 with $\nu = 10^{-6}$. Solver times with Pardiso for polynomial degree $k = 2$ (left), $k = 3$ (center), and $k = 4$ (right), $\delta = 1$ (skew-symmetric case).

system, possibly of saddle point type. Constructions of the basis for arbitrary polynomial degree in two and three space dimensions for simplicial meshes were provided. Other algorithmic issues, like the incorporation of non-homogeneous Dirichlet boundary conditions and the computation of a finite element pressure approximation were addressed and corresponding algorithms were proposed. The finite element error analysis for the velocity from [22] carries over to the proposed method and an estimate for the gradient of the pressure error was derived. Numerical studies showed the expected orders of convergence. Using a sparse direct solver, the proposed methods proved to be consistently faster than the full mixed methods from [22] and in some situations even more efficient than the reduced mixed methods derived in [22].

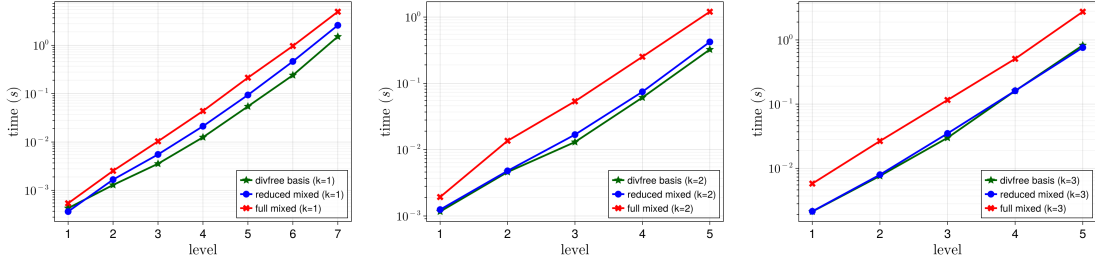


Fig. 9: Example 6.1 with $\nu = 10^{-6}$. Solver times with Pardiso for polynomial degree $k = 1$ (left), $k = 2$ (center), and $k = 3$ (right), $\delta = -1$ (symmetric case).

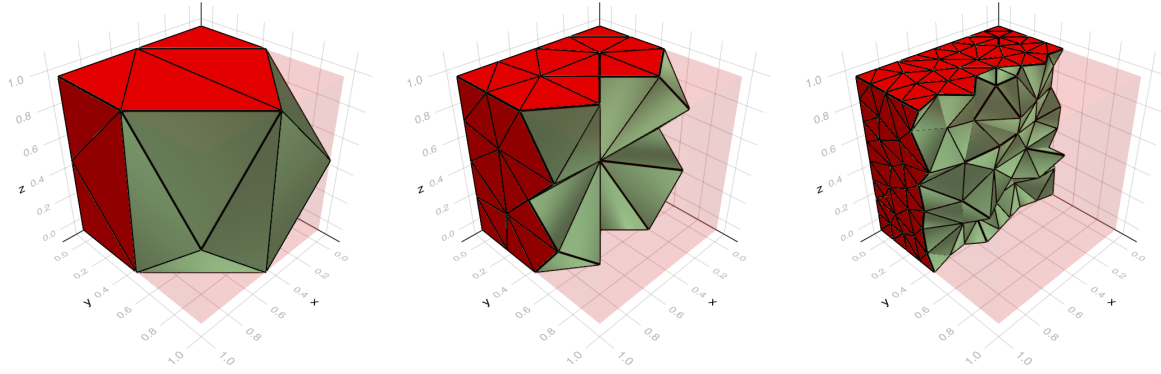


Fig. 10: Example 6.2. Slices of the three coarsest computational grids.

Table 3: Example 6.2. Number of degrees of freedom (ndofs) and number of non-zero sparse matrix entries (nnz) of the full system for the decoupled method with divergence-free basis (dfb) and the reduced mixed method (red) for different degrees k and $\delta = 1$ (skew-symmetric case).

level	ndofs dfb (k=2)	ndofs red (k=2)	nnz dfb (k=2)	nnz red (k=2)
1	277	259	15134	18933
2	1312	1239	94027	135001
3	8647	8339	756249	1190877
4	52994	51805	5028568	8308893
level	ndofs dfb (k=3)	ndofs red (k=3)	nnz dfb (k=3)	nnz red (k=3)
1	640	622	64883	58728
2	3262	3189	395725	350243
3	23161	22853	3260511	2882731
4	147080	145891	22085754	19540909

The extension of the proposed methods to the incompressible Navier–Stokes equations can be performed along the lines of [2], i.e., special discrete forms of the nonlinear convective term have to be considered. A further aspect of interest is the efficiency of the methods, in particular in comparison with the reduced mixed methods from [22], if appropriate iterative solvers for the arising linear systems of equations are applied.

Table 4: Example 6.2. Number of degrees of freedom (ndofs) and number of non-zero sparse matrix entries (nnz) of the full system for the decoupled method with divergence-free basis (dfb) and the reduced mixed method (red) for different degrees k and $\delta = -1$ (symmetric case).

level	ndofs dfb (k=1)	ndofs red (k=1)	nnz dfb (k=1)	nnz red (k=1)
1	100	82	2469	784
2	442	369	14833	5195
3	2737	2429	124101	46959
4	16334	15145	824112	327725
5	109681	104831	5886385	2412889

level	ndofs dfb (k=2)	ndofs red (k=2)	nnz dfb (k=2)	nnz red (k=2)
1	277	259	15254	19067
2	1312	1239	94053	135001
3	8647	8339	756255	1190877
4	52994	51805	5028578	8308893

level	ndofs dfb (k=3)	ndofs red (k=3)	nnz dfb (k=3)	nnz red (k=3)
1	640	622	65431	58728
2	3262	3189	398321	350243
3	23161	22853	3280405	2882731
4	147080	145891	22211122	19540909

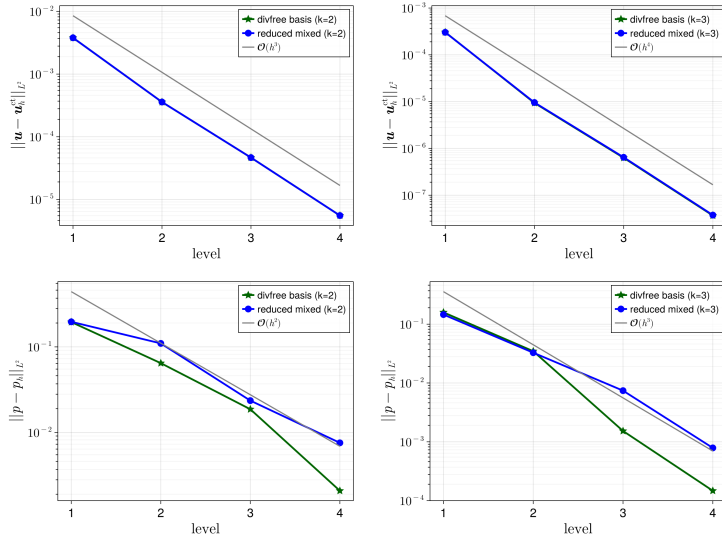


Fig. 11: Example 6.2. $L^2(\Omega)$ velocity error (top) and pressure error (bottom) for the polynomial degree $k = 2$ (left) and $k = 3$ (right), $\delta = 1$ (skew-symmetric case).

REFERENCES

- [1] N. AHMED, G. R. BARRENECHEA, E. BURMAN, J. GUZMÁN, A. LINKE, AND C. MERDON, *A pressure-robust discretization of Oseen's equation using stabilization in the vorticity equation*, SIAM J. Numer. Anal., 59 (2021), pp. 2746–2774.
- [2] N. AHMED, V. JOHN, X. LI, AND C. MERDON, *Inf-sup stabilized Scott-Vogelius pairs on general shape-regular simplicial grids for Navier-Stokes equations*, Comput. Math. Appl., 168 (2024), pp. 148–161.
- [3] D. N. ARNOLD, F. BREZZI, B. COCKBURN, AND L. D. MARINI, *Unified analysis of discontinuous Galerkin methods for*

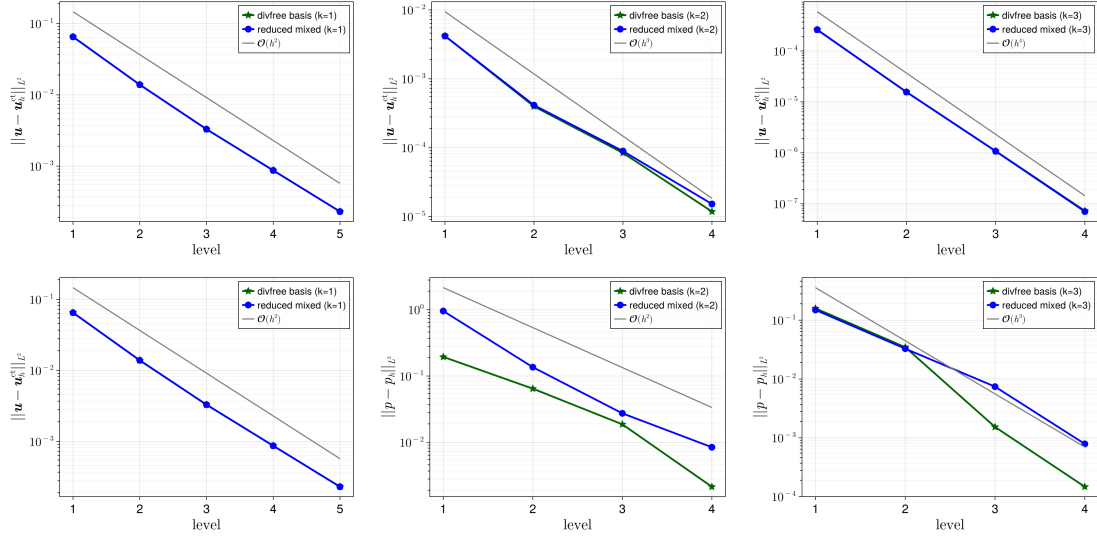


Fig. 12: Example 6.2. $L^2(\Omega)$ velocity error (top) and pressure error (bottom) for the polynomial degree $k = 1$ (left), $k = 2$ (center), and $k = 3$ (right), $\delta = -1$ (symmetric case).

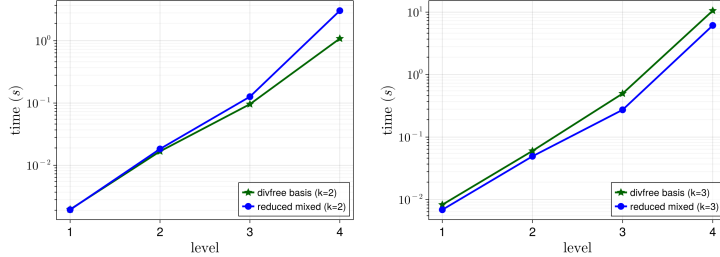


Fig. 13: Example 6.2. Solver times with Pardiso for polynomial degree $k = 2$ (left) and $k = 3$ (right), $\delta = 1$ (skew-symmetric case).

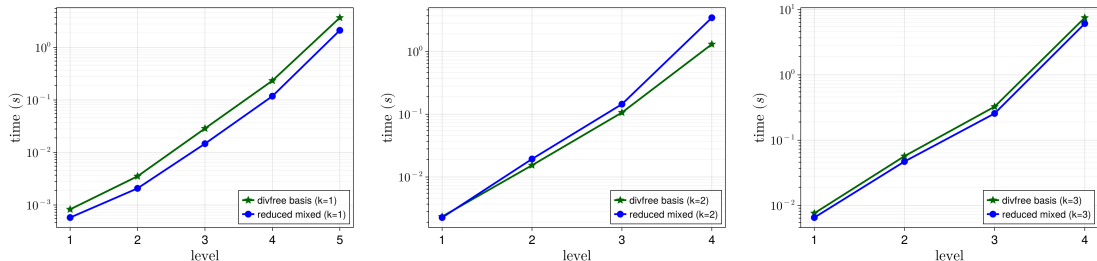


Fig. 14: Example 6.2. Solver times with Pardiso for polynomial degree $k = 1$ (left), $k = 2$ (center), and $k = 3$ (right), $\delta = -1$ (symmetric case).

elliptic problems, SIAM J. Numer. Anal., 39 (2002), pp. 1749–1779.

[4] D. N. ARNOLD, R. S. FALK, AND R. WINTHER, *Preconditioning in $H(\text{div})$ and applications*, Math. Comp., 66 (1997), pp. 957–984.

[5] D. N. ARNOLD AND J. QIN, *Quadratic velocity/linear pressure Stokes elements*, Advances in Computer Methods for Partial Differential Equations-VII, R. Vichnevetsky, D. Knight & G. Richter, eds., IMACS, New Brunswick, NJ, (1992), pp. 28–34.

[6] C. BERNARDI AND G. RAUGEL, *Analysis of some finite elements for the Stokes problem*, Math. Comp., 44 (1985), pp. 71–79.

[7] D. BOFFI, F. BREZZI, AND M. FORTIN, *Mixed finite element methods and applications*, vol. 44 of Springer Series in Computational Mathematics, Springer, Heidelberg, 2013.

[8] S. C. BRENNER AND L. R. SCOTT, *The mathematical theory of finite element methods*, vol. 15 of Texts in Applied Mathematics, Springer, New York, third ed., 2008.

[9] E. A. CARLSSON, KRISTOFFER, *Pardiso.jl*, (2025). Julia package, version 1.0.1.

[10] V. DECARIA, W. LAYTON, AND M. McLAUGHLIN, *A conservative, second order, unconditionally stable artificial compression method*, Comput. Methods Appl. Mech. Engrg., 325 (2017), pp. 733–747.

[11] G. FU, *An explicit divergence-free DG method for incompressible flow*, Comput. Methods Appl. Mech. Engrg., 345 (2019), pp. 502–517.

[12] B. GARCÍA-ARCHILLA, V. JOHN, AND J. NOVO, *On the convergence order of the finite element error in the kinetic energy for high Reynolds number incompressible flows*, Comput. Methods Appl. Mech. Engrg., 385 (2021), pp. Paper No. 114032, 54.

[13] V. GIRAUT AND P.-A. RAVIART, *Finite element methods for Navier–Stokes equations*, vol. 5 of Springer Series in Computational Mathematics, Springer-Verlag, Berlin, 1986. Theory and algorithms.

[14] J. GUERMOND, P. MINEV, AND J. SHEN, *An overview of projection methods for incompressible flows*, Comput. Methods Appl. Mech. Engrg., 195 (2006), pp. 6011–6045.

[15] J. GUERMOND AND J. SHEN, *A new class of truly consistent splitting schemes for incompressible flows*, J. Comput. Phys., 192 (2003), pp. 262–276.

[16] J.-L. GUERMOND AND P. MINEV, *High-order time stepping for the incompressible Navier–Stokes equations*, SIAM J. Sci. Comput., 37 (2015), pp. A2656–A2681.

[17] J.-L. GUERMOND AND P. MINEV, *High-order adaptive time stepping for the incompressible Navier–Stokes equations*, SIAM J. Sci. Comput., 41 (2019), pp. A770–A788.

[18] J. L. GUERMOND AND J. SHEN, *Velocity-correction projection methods for incompressible flows*, SIAM J. Numer. Anal., 41 (2003), pp. 112–134.

[19] F. HUANG AND J. SHEN, *Stability and error analysis of a second-order consistent splitting scheme for the Navier–Stokes equations*, SIAM J. Numer. Anal., 61 (2023), pp. 2408–2433.

[20] V. JOHN, *Finite element methods for incompressible flow problems*, vol. 51 of Springer Series in Computational Mathematics, Springer, Cham, 2016.

[21] V. JOHN, X. LI, AND C. MERDON, *Pressure-robust $L^2(\Omega)$ error analysis for Raviart–Thomas enriched Scott–Vogelius pairs*, Applied Mathematics Letters, 156 (2024), p. 109138.

[22] V. JOHN, X. LI, C. MERDON, AND H. RUI, *Inf-sup stabilized Scott–Vogelius pairs on general shape-regular simplicial grids by Raviart–Thomas enrichment*, Math. Models Methods Appl. Sci., 34 (2024), pp. 919–949.

[23] V. JOHN, A. LINKE, C. MERDON, M. NEILAN, AND L. G. REBHOLZ, *On the divergence constraint in mixed finite element methods for incompressible flows*, SIAM Rev., 59 (2017), pp. 492–544.

[24] P. L. LEDERER, A. LINKE, C. MERDON, AND J. SCHÖBERL, *Divergence-free reconstruction operators for pressure-robust Stokes discretizations with continuous pressure finite elements*, SIAM J. Numer. Anal., 55 (2017), pp. 1291–1314.

[25] X. LI AND H. RUI, *A low-order divergence-free $H(\text{div})$ -conforming finite element method for Stokes flows*, IMA J. Numer. Anal., 42 (2021), pp. 3711–3734.

[26] X. LI AND J. SHEN, *Unconditionally stable consistent splitting schemes for the Navier–Stokes equations with c^0 finite elements*, Math. Comp., (2025). Published electronically.

[27] J.-G. LIU, J. LIU, AND R. L. PEGO, *Stability and convergence of efficient Navier–Stokes solvers via a commutator estimate*, Communications on Pure and Applied Mathematics, 60 (2007), pp. 1443–1487.

[28] C. M. MERDON AND E. A. JAAP, PATRICK, *ExtendableFEM.jl*, (2025). Julia package, version 1.3.0.

[29] L. MU, J. WANG, X. YE, AND S. ZHANG, *A discrete divergence free weak Galerkin finite element method for the Stokes equations*, Appl. Numer. Math., 125 (2018), pp. 172–182.

[30] R. SCHEICHL, *Decoupling three-dimensional mixed problems using divergence-free finite elements*, SIAM J. Sci. Comput., 23 (2002), pp. 1752–1776.

[31] O. SCHEK, K. GÄRTNER, W. FICHTNER, AND A. STRICKER, *PARDISO: a high-performance serial and parallel sparse linear solver in semiconductor device simulation*, Future Gener. Comput. Syst., 18 (2001), pp. 69–78.

[32] P. W. SCHROEDER, C. LEHRENFELD, A. LINKE, AND G. LUBE, *Towards computable flows and robust estimates for inf-sup stable FEM applied to the time-dependent incompressible Navier–Stokes equations*, SeMA J., 75 (2018), pp. 629–653.

[33] L. R. SCOTT AND M. VOGELIUS, *Conforming finite element methods for incompressible and nearly incompressible continua*, in Large-scale computations in fluid mechanics, Part 2 (La Jolla, Calif., 1983), vol. 22 of Lectures in

Appl. Math., Amer. Math. Soc., Providence, RI, 1985, pp. 221–244.

[34] L. R. SCOTT AND M. VOGELIUS, *Norm estimates for a maximal right inverse of the divergence operator in spaces of piecewise polynomials*, ESAIM Math. Model. Numer. Anal. - Modélisation Mathématique et Analyse Numérique, 19 (1985), pp. 111–143.

[35] J. SHEN, *On error estimates of projection methods for Navier–Stokes equations: First-order schemes*, SIAM J. Numer. Anal., 29 (1992), pp. 57–77.

[36] J. WANG, Y. WANG, AND X. YE, *A robust numerical method for Stokes equations based on divergence-free $H(\text{div})$ finite element methods*, SIAM J. Sci. Comput., 31 (2009), pp. 2784–2802.

[37] X. YE AND C. A. HALL, *A discrete divergence-free basis for finite element methods*, Numer. Algo., 16 (1997), pp. 365–380.

[38] S. ZHANG, *A new family of stable mixed finite elements for the 3D Stokes equations*, Math. Comp., 74 (2005), pp. 543–554.